

Chemical Space-Informed Machine Learning Models for Rapid Predictions of X-ray Photoelectron Spectra of Organic Molecules

Susmita Tripathy,¹ Surajit Das,¹ Shweta Jindal,¹ and Raghunathan Ramakrishnan^{1, a)}

Tata Institute of Fundamental Research, Hyderabad 500046, India

(Dated: 16 August 2024)

We present machine learning models based on kernel-ridge regression for predicting X-ray photoelectron spectra of organic molecules originating from the K -shell ionization energies of carbon (C), nitrogen (N), oxygen (O), and fluorine (F) atoms. We constructed the training dataset through high-throughput calculations of K -shell core-electron binding energies (CEBEs) for 12,880 small organic molecules in the bigQM7 ω dataset, employing the Δ -SCF formalism coupled with meta-GGA-DFT and a variationally converged basis set. The models are cost-effective, as they require the atomic coordinates of a molecule generated using universal force fields while estimating the target-level CEBEs corresponding to DFT-level equilibrium geometry. We explore transfer learning by utilizing the atomic environment feature vectors learned using a graph neural network framework in kernel-ridge regression. Additionally, we enhance accuracy within the Δ -machine learning framework by leveraging inexpensive baseline spectra derived from Kohn–Sham eigenvalues. When applied to 208 combinatorially substituted uracil molecules larger than those in the training set, our analyses suggest that the models may not provide quantitatively accurate predictions of CEBEs but offer a strong linear correlation relevant for virtual high-throughput screening. We present the dataset and models as the Python module, `cebeconf`, to facilitate further explorations.

Keywords: X-ray photoelectron spectra, core-electron binding energy, density functional theory, machine learning, chemical space

I. INTRODUCTION

X-ray photoelectron spectroscopy (XPS) distinguishes atoms based on the ionization energies of their core electrons effectively screened by molecular valence electrons. The resulting chemical shifts of core-electron binding energies (CEBEs) enable the identification of the local bonding environment of an atom. A typical XPS spectrum comprises peaks; some merged to form a broader distribution, corresponding to ionized core electrons detected experimentally as photocurrent¹. The positions and intensities of an XPS spectrum can provide insights on molecular internal coordinates², orientation of adsorbates relative to the substrate³, chemical composition^{4,5}, as well as physical conditions such as temperature^{3,4} and pressure⁵.

Advancements in modern synchrotron sources have enabled the precise detection of chemical shifts of CEBEs, achieving a resolution of 0.05 eV⁶. The precision of $1s$ -CEBEs (denoted hitherto E_b^{1s}) in atoms is limited by lifetime broadening. XPS achieves a precision of 0.1 eV for $1s$ -CEBEs of carbon (C) atoms in molecules⁷. For nitrogen (N) and oxygen (O), peak widths of 0.13 and 0.16 eV, respectively, are commonly used in spectral deconvolution⁷, often corroborated by theoretical peak assignments⁴. Theoretical CEBEs of even semi-quantitative accuracy can aid experimental XPS assignment^{8,9}, thereby contributing to diverse applications such as structure elucidation³, catalysis^{10,11},

characterization of energy storage materials¹², and material composition analysis⁸,

For achieving quantitatively accurate theoretical predictions of XPS, it is crucial to account for core-orbital relaxation effects, which unfold at a sub-femtosecond ($< 10^{-15}$ s) timescale mirroring the ultrafast temporal dynamics during experimental detection, resonating with the energy-time uncertainty principle^{1,13}. CEBEs estimated using molecular orbital (MO) energies—based on the Koopmans’ approximation^{8,14} in density functional theory (DFT)—show large errors due to the lack of core relaxation in MOs that determine the ground state electronic density^{15,16}. Many-body methods such as GW approximation¹⁷, which utilizes Green’s function (G) and a screened Coulomb interaction (W), and random phase approximation¹⁸ adequately address screening effects. While these methods provide robust frameworks, their computational complexity prohibits their application for large-scale data generation. Within DFT, alternative approaches such as the Slater transition state method^{19,20} and the Δ -self consistent field (Δ -SCF) approach^{21–23} offer promising avenues for incorporating orbital relaxation effects. These methods explicitly account for the vacancy in a core-orbital—*i.e.*, hole—using charge-constraining algorithms such as the maximum-overlap-method²⁴, thereby preventing the variational collapse of non-Aufbau Slater determinants. While the numerical convergence²⁵ of Δ -SCF is highly coupled to the choice of projectors used for wavefunction localization^{26,27}, it emerges as the best option in terms of the overall efficiency^{26,28}.

The magnitude of E_b^{1s} of an element in its reduced state is lower than its oxidized states. For example, the

^{a)}Electronic mail: ramakrishnan@tifrh.res.in

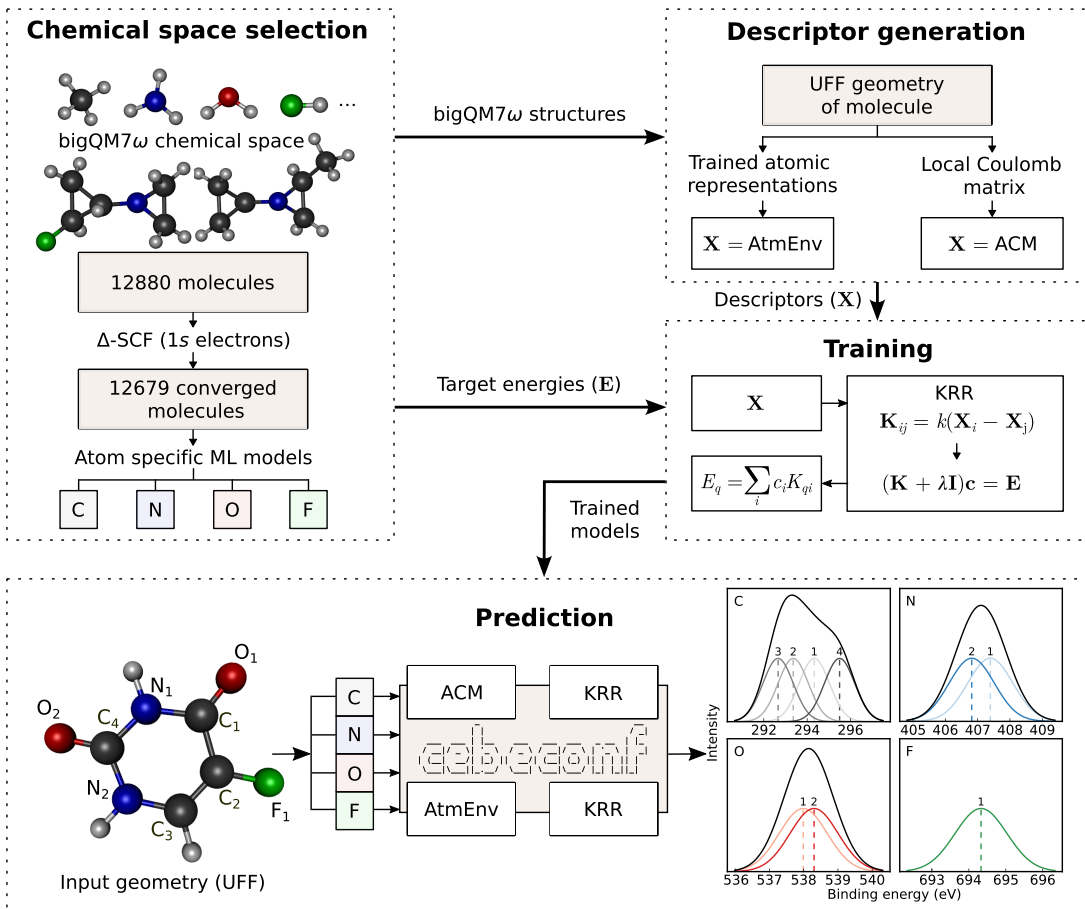


FIG. 1. Workflow of the study: (i) For 85,837 C, O, N, or F atoms in 12,679 molecules of the bigQM7 ω chemical space, Δ -SCF calculations were performed to calculate 1s-CEBEs. (ii) Structure-based descriptors—atomic environment from graph neural networks (AtmEnv) and atomic Coulomb matrix (ACM)—were generated using molecular geometries calculated with UFF. (iii) For each main-group element, kernel-ridge-regression models were created using 80% of the data. (iv) Trained models are shared through the `cebebconf` module²⁹ that requires UFF-level molecular geometry as the input for new predictions.

E_b^{1s} (C) of a CH moiety is approximately 285 eV³⁰, which, with the introduction of electronegative substituents as in CF, CF₂, CF₃, and CF₃OH is systematically shifted to 288, 291, 293.5, and 295 eV, respectively⁶. XPS measurements of fluorinated polyethylenes reveal similar trends³¹. These systematic variations in E_b^{1s} with chemical composition reveal a clear correlation between this quasi-atomic property and the local environment of an atom in a molecule. The formal existence of this structural-property relationship is a crucial prerequisite for ML modeling based on structure-based descriptors, as it ensures that the models can reliably leverage structural information to predict XPS spectra.

Molecular chemical space datasets, such as QM9³² and bigQM7 ω ³³ have facilitated the elucidation of structure-property relationships through machine learning (ML) modeling³⁴. The Δ -ML³⁵ approach further enhances the accuracy by utilizing inexpensive baseline methods^{36–38}. In recent years, ML models have successfully predicted local properties of atoms-in-molecules (AIM) such as nuclear magnetic resonance (NMR) shield-

ing parameters^{36,39–41} and acid dissociation constants (pKa)^{40,41}, as well as ‘global’ molecular properties such as atomization energies³², electronic excitation energies in ultraviolet (UV)-visible spectroscopy^{33,42,43}, or frontier MO energy gaps⁴⁴, demonstrating the effectiveness of ML-aided computational chemistry endeavors⁴⁵. ML techniques have found utility in spectroscopic applications for mapping spectroscopic features to structural motifs^{46,47}. Specifically, several studies^{38,48,49} have explored the prediction of XPS spectra in materials. In the context of XPS spectra for gas-phase molecules, Rupp *et al.*³⁴ investigated a subset of QM9 with the stoichiometry C₇H₁₀O₂, consisting of 6095 constitutional isomers, while Golze *et al.*³⁸ focused on a QM9 subset containing only H, C, and O atoms. Although the inclusion of additional elements in the training data can reduce the accuracy of ML models, it also enhances their generality. Therefore, we include all CONF atoms from the bigQM7 ω dataset, incorporating greater diversity into our training data. The present study explores data-driven modeling of XPS spectra of small organic molecules. We select the new

chemical space dataset, bigQM7 ω ³³, which has a larger number of molecules containing upto 7 CONF atoms than the corresponding subset of QM9, offering greater structural and compositional diversity. The minimum energy structures in bigQM7 ω were calculated using the range-separated hybrid DFT method ω B97XD⁵⁰, thereby enhancing the quality of structures suitable for developing datasets of various properties in a single-point fashion. We present ML models for predicting the XPS spectra of organic molecules at the Δ -SCF level, trained using structural descriptors derived from inexpensive geometries obtained with the universal force field (UFF)⁵¹. Previous studies have explored the use of cost-effective baseline-level geometries for out-of-sample predictions without a significant loss in accuracy^{35,45}. By using UFF-level geometries, we eliminate the need for computationally expensive DFT-level geometries, making the XPS calculations for new ML predictions more efficient. These inexpensive inputs are used to generate lightweight descriptors obtained from graph neural networks (GNNs) and a local version of the Coulomb matrix (CM) descriptor^{34,52}. Further, we propose using Kohn–Sham (KS) eigenvalues obtained from single-point calculations of neutral molecules as a baseline in Δ -ML. FIG. 1 illustrates our data generation and ML workflow. The trained models are packaged within the Python module `cebeconf`²⁹, providing easy access for XPS predictions.

In the following, IIA compiles details of electronic structure calculations. In IIB, we discuss a scheme to assign quasi-particle energies to CEBEs based on the Mulliken population scheme. We describe the details of ML for modeling local atomic properties in IIC. In IID, we gather the details of atomic descriptors. We present our results in III: Evaluation of the DFT method used for data generation (III A); property trends and data distribution (III B); and analysis of the performance of ML models (III C and III D). We highlight the transferability of our models by applying them to a class of biomolecules in III E. Finally, we conclude in section IV, highlighting the features of the ML models presented in this study and their scope for future applications.

II. METHODOLOGY

A. Electronic structure calculations

We performed electronic structure calculations using the all-electron, numerically tabulated atom-centered orbital (NAO) code, FHI-aims⁵³. For training the ML models reported in this study, we selected the bigQM7 ω dataset, which has been used for generating datasets of electronic excitation spectra^{33,54}. The molecular structures in bigQM7 ω were optimized in the original study³³ using the ConnGO approach that preserves the covalent bond connectivities during geometry optimization⁵⁵. For this purpose, the range-separated hybrid DFT method, ω B97XD, was used in combination

with the def2TZVP basis set. Since the change in nuclear coordinates have negligible effects on XPS, the minimum energy geometries of neutral ground states were used in all calculations.

For Δ -SCF calculations, we selected the meta-generalized gradient approximation (mGGA) to DFT, SCAN, along with the Tight-Full, basis set. The 1s-CEBE (E_b^{1s}) in a Δ -SCF calculation is obtained by subtracting the total energy of the neutral molecule (E_{mol}) from that of the corresponding 1s core-ionized cation (E_{cation}^{1s})

$$E_b^{1s} = E_{\text{cation}}^{1s} - E_{\text{mol}}. \quad (1)$$

We exclusively use NAOs with ‘tight’ integration grids to accurately account for orbital relaxation effects in the cationic states involved in the Δ -SCF calculations. While ‘tight’ settings in FHI-aims have ‘tier 2’ basis functions as default, we selected the highest ‘tier’ possible for each element, *i.e.*, ‘tier 3’ for hydrogen (H) and beyond ‘tier 4’ for CONF atoms. We refer to this basis set as Tight-Full. We have also probed the valence-correlation consistent NAO, NAO-VCC-5Z, which is analogous to Dunning’s cc-pV5Z⁵⁶. Since there is minimal error for core-levels when using large basis sets, core augmentation functions^{20,57} were not utilized.

Holes at core-levels were constrained using the `force_occupation_basis` keyword in FHI-aims. The corresponding approach is a variant of the maximum overlap method²⁴, specifying the hole in a quasi-AO⁵⁸. One can also use the `force_occupation_projector`, which directly constrains the hole at a specified MO; however, we found the former to be more variationally stable²⁶ making it suitable for automated high-throughput calculations with minimal manual data curation.

Intricate modifications specific to core-level predictions are avoided in the Koopmans’ approximation. Accordingly, the negative of the KS orbital energy, ε_i , approximates the 1s-CEBE^{14,26}

$$E_b^{1s} \approx -\varepsilon_{1s}. \quad (2)$$

In this work, we performed single point calculations with the PBE-DFT method and the cc-pVDZ basis set to calculate ε_{1s} using UFF-level structures obtained using the program Openbabel⁵⁹. Despite lacking contributions from orbital relaxation effects in the Koopmans’ interpretation^{15,60}, its relative ease of use makes it an efficient choice as a baseline method in Δ -ML.

GW method is considered the ‘‘gold standard’’ for modeling CEBEs^{38,61}. In particular, the contour deformation to evaluate self energy in GW , improves the quasi-particle energies for core-levels^{62,63}. Among presently available GW approximations, Hedin shifted GW , $G_{\Delta H}W_0$, which introduces a state-specific global shift in the quasiparticle self-consistent equations is the most accurate⁶¹. Hence, in this study we use $G_{\Delta H}W_0$ for evaluating the accuracy of Δ -SCF results. In all

GW calculations, we used KS-eigenstates obtained using PBE-DFT with cc-pVnZ (n=T,Q,5) basis sets and extrapolated the results to arrive at the basis limit values, following the procedure previously used by Golze *et al.*^{63,64}. For systems exhibiting non-monotonic convergence with basis set size, due to contraction errors⁶⁵, we used cc-pV5Z values instead of extrapolated energies. The computational complexity of *GW* methods, which increases manifold with basis set size limits its applicability in high-throughput data generation. Therefore, *GW* calculations were performed only for a small subset of bigQM7 ω . We use *GW*-predicted E_b^{1s} for assessing the accuracy Δ -SCF and Koopmans’ approximations based on the mGGA-DFT methods, SCAN and TPSS.

In our calculations, 219 1s-core-ionized cations did not achieve density convergence during the SCF procedure. These atoms belong to 201 molecules, which have been excluded from the dataset of 12,880 molecules. An analysis of these 201 molecules indicates that all of them that experienced convergence failure contain at least one double bond. While the corresponding atoms are not necessarily sp^2 hybridized in every instance, double bonds generally contribute to convergence difficulties and are the most common issue among each atom type when classified by hybridization. The remaining molecules exhibiting convergence failure contain a carbonyl group. The distribution of these non-converged systems is detailed in Table S5 of the SI. SMILES entries for all molecules exhibiting SCF convergence failure are listed in Table S6 of the SI. While such calculations can be converged through careful assessments of numerical criteria and localization procedures²⁸, we excluded these molecules for the sake of consistent numerical settings across the dataset.

The resulting XPS dataset consists of 85837 entries of E_b^{1s} of the constituent CONF atoms of 12679 molecules obtained using Δ -SCF with the SCAN/Tight-Full method. From this dataset, shuffled train-test splits of various sizes were selected for training the ML models. Further, to validate the ML models, we explore combinatorially substituted derivatives of pyrimidinones and uracil, resulting in 208 biomolecules. For this set, we have calculated E_b^{1s} at the SCAN/Tight-Full level using minimum energy structures determined using the ω B97XD/def2TZVP method as implemented in Gaussian16⁶⁶. Further, for the validation set, we have calculated Koopmans’ estimations with the PBE/cc-pVDZ method using geometries determined with UFF. In all calculations, we accounted for relativistic effects through the atomic zeroth-order regular approximation (aZORA)^{26,67}. When using the Δ -ML models presented in this study for new predictions, along with UFF geometry, it is necessary to provide the baseline CEBEs, which are the PBE/cc-pVDZ Koopmans’ estimates determined using UFF geometry. Since the effect of aZORA on CEBEs results in a constant shift, non-relativistic PBE/cc-pVDZ values can be corrected *a posteriori*^{23,61,64,68} by adding 0.29, 0.55, 0.97, or 1.57 eV for C, O, N, or F atoms, respectively. Further details are

provided in Figure S1 of the SI.

B. Assignment of quasi-particle energy to CEBE

The localization of core-holes is assumed inherently in XPS. However, vibronic fine structure underlying the XPS spectrum sheds insights on the participation of core-level MOs in very-weak bonding^{69,70}. These splittings can be of the order of milli-eVs and observed in high-precision spectroscopic techniques. Dispersions in CEBEs for chemically equivalent atoms in symmetric molecules such as benzene⁷⁰, acetylene⁶⁹, dinitrogen⁷¹, and others⁷² have been observed. Splittings arising from the coupling of core-levels can also be observed and identified in the one-particle energies obtained from KS-eigenvalues. Experimentally, in the case of benzene, 6 degenerate core levels lead to 4 energy levels spanning a range of 64 meV⁷⁰(see Table S1 of SI). While by definition, the values of E_b^{1s} of identical atoms will be similar in Δ -SCF predictions, dispersions in E_b^{1s} are captured in quasiparticle energies. Therefore, to map the quasiparticle energies of MOs to the respective Δ -SCF energies for use as a baseline in Δ -ML, we use Mulliken population analysis⁵⁸.

For assigning the k -th MO to an AO centered on atom A , of angular momentum quantum number l , we use Mulliken population projected on the MO defined as

$$P_{A,k,l}^M = 2 \sum_{\mu \in A, \mu \in l} \sum_{\lambda} C_{\mu,k} C_{\lambda,k} S_{\lambda,\mu}. \quad (3)$$

Here, the summation is performed over all AOs, μ , centered on atom A with angular momentum l . Here, $C_{\mu,k}$ and $C_{\lambda,k}$ are elements of the k -th KS eigenvector corresponding to the AOs, μ and λ , respectively. Further, $S_{\lambda,\mu}$ is an element of the overlap or inner product matrix in the AO representation. For a given k , the CEBE corresponds to the atom with a maximal projected population. Consequently, when the population is identical for symmetrically equivalent atoms, they will be assigned the same quasiparticle energy. In the bigQM7 ω dataset, using KS eigenvalues at the PBE/cc-pVDZ level, 79 pairs of chemically equivalent atoms were assigned the same KS-eigenvalue in 59 molecules.

C. KRR-ML framework for modeling CEBE

KRR is an efficient ML framework for accurately modeling molecular and materials properties^{52,73,74}. It also facilitates modeling local quasi-atomic properties in molecules such as NMR shielding, CEBE, and partial charges on atoms^{34,36}. In this study, we apply KRR-ML for modeling E_b^{1s} . An attractive feature of KRR is that the training, *i.e.*, the model optimization, is performed by minimizing a convex function for which direct linear solvers such as Cholesky decomposition or matrix inver-

sion yield numerically exact solution within the limits of numerical precision^{45,75}. Accordingly, the regression coefficients are obtained by solving the following equation.

$$[\mathbf{K} + \lambda\mathbf{I}] \mathbf{c} = \mathbf{E}_b^{1s}, \quad (4)$$

where \mathbf{K} and \mathbf{I} are $N \times N$ kernel and identity matrices, respectively, while \mathbf{E}_b^{1s} is the vector of CEBE values of N training entities. The kernel matrix element, K_{ij} , captures the similarity between two training atoms (i and j) in the form of a kernel function, k , sometimes referred as radial basis functions (RBFs) of the corresponding descriptors, $k(\mathbf{d}_i, \mathbf{d}_j) = k(\mathbf{d}_i - \mathbf{d}_j)$. For brevity, we define $\mathbf{d}_i - \mathbf{d}_j$ as D_{ij} . The choice of the descriptor or the representation vector, \mathbf{d} , is presented in IID.

In this study, we explore Laplacian (a.k.a. exponential) and Gaussian kernels defined as

$$\begin{aligned} k^{\text{Laplacian}}(D_{ij}) &= \exp(-\|D_{ij}\|_1/\sigma) \text{ and} \\ k^{\text{Gaussian}}(D_{ij}) &= \exp(-\|D_{ij}\|_2^2/2\sigma^2). \end{aligned} \quad (5)$$

The Laplacian kernel depends on the L_1 norm, a.k.a. taxicab norm defined as $\|\mathbf{x}\|_1 = \sum_i |x_i|$, whereas the Gaussian kernel uses the Euclidean norm defined as $\|\mathbf{x}\|_2 = \sqrt{\sum_i x_i^2}$. There are other definitions of kernels where the pairwise comparison can also be an inner-product⁷⁵, which we do not explore in this study.

For a query atom, q , KRR-ML predicts E_b^{1s} according to the following equation.

$$E_b^{1s}(q) \approx \sum_{i=1}^N c_i K_{qi}, \quad (6)$$

where the summation on the right side is performed over N training examples, c_i are the regression coefficients obtained through training and K_{qi} is the kernel matrix element evaluated between the query atom q and training atom i .

The hyperparameters, λ (in Eq. 4) and σ (in Eq. 5), modulate the performance of KRR-ML models. The parameter λ is a non-negative real number serving two purposes⁴⁵. For positive values, it introduces a penalty to regularize the magnitudes of the regression coefficients, which is necessary to decrease the impact of outliers on the model’s performance. Another more common scenario is that there are redundancies in the training set. For instance, training examples i and j are the same resulting in two identical rows and columns in of \mathbf{K} , which becomes a singular matrix. In such cases, adding the second term, $\lambda\mathbf{I}$, conditions the linear system defined in Eq. 4. It is important to note that the aforementioned redundancies can occur if the representations lack uniqueness, even for a few training examples. In anticipation of such linear dependencies, in all KRR-ML calculations, we set λ as 10^{-4} .

The kernel width, σ , determines the width of the kernel-RBFs, thereby governing the spread over training examples for predictions. In a previous work⁷⁶, a

heuristic approach was proposed to determine σ by setting the minimum of the off-diagonal elements of \mathbf{K} to $1/2$, $K_{ij}^{\min} = 1/2$, as a measure of conditioning \mathbf{K} . Accordingly, σ can be determined using the maximal value of D_{ij} over a random sample. For Laplacian and Gaussian kernels, one arrives at^{45,76}:

$$\sigma_{\text{opt}}^{\text{Laplacian}} = \frac{D_{ij}^{\max}}{\log 2}; \quad \sigma_{\text{opt}}^{\text{Gaussian}} = \frac{D_{ij}^{\max}}{\sqrt{2 \log 2}}. \quad (7)$$

Since descriptor differences have non-trivial distributions, for KRR-ML modeling of NMR shielding in the QM9-NMR dataset³⁶, better results were reported when using the median of the descriptor differences instead of D_{ij}^{\max} .

To shed more light on the optimal value of kernel-width for a given target property, we set K_{ij}^{\min} to be free parameter, $0 < \tau < 1$, and determine σ as follows:

$$\sigma_{\text{opt}}^{\text{Laplacian}} = \frac{D_{ij}^{\max}}{\log 1/\tau}; \quad \sigma_{\text{opt}}^{\text{Gaussian}} = \frac{D_{ij}^{\max}}{\sqrt{2 \log 1/\tau}}. \quad (8)$$

We scanned τ in the range 0.03 to 0.99 in steps of 0.03.

D. Local descriptors for atom-in-molecules

ML-based modeling of local properties of atoms-in-molecules such as CEBEs presents distinct challenges compared to global molecular or material properties. One of the primary difficulties lies in the lack of specialized structural descriptors tailored for these local properties. Traditional descriptors are designed to capture the overall molecular geometry and are unsuitable for modeling local atomic environments. Additionally, local properties are highly sensitive to subtle changes in the chemical environment, necessitating models that can capture intricate variations at the atomic level. Consequently, more extensive benchmarking of ML strategies is essential to improve the modeling of CEBEs. For ML modeling of local properties with KRR, several descriptors or representations have been proposed to describe the atomic environment: Gaussian RBFs⁷⁷, local CM⁵², smooth overlap of atomic positions (SOAP)⁷⁸, neural network (NN) embeddings⁷⁹, atomic spectral London-Axilrod-Teller-Muto (aSLATM)⁸⁰, and Faber-Christensen-Huang-Lilienfeld (FCHL)⁸¹. Formally, many-body RBFs, SOAP, aSLATM, and FCHL are continuous representations placing heavy storage requirements. On the other hand, CM and embeddings are discrete representations amenable to rapid predictions. Since one of the aims of this study is to present ML models pre-trained on a large training set, we have explored atomic CM (ACM) and atomic environment obtained as embeddings by training a GNN (AtmEnv).

As stated before, of the 12,880 molecules in the bigQM7 ω dataset, 201 did not converge during Δ -SCF calculations. The remaining 12,679 were partitioned

into four subsets based on the presence of C/O/N/F atoms. The subset with ‘C’ was the largest, with 12674 molecules, as ‘C’ is present in all molecules in bigQM7 ω but HF, H₂O, NH₃, F₂, and O₂. See Table S2 of SI for further details.

The target property, E_b^{1s} of C/O/N/F atoms were calculated using the minimum energy geometries of the bigQM7 ω molecules, previously determined at the ω B97XD/def2TZVP level of theory³³. However, to generate local descriptions, we utilize molecular geometries determined using UFF starting from ‘simplified molecular-input line-entry system’ (SMILES) strings. As in previous studies^{35,43}, ML models trained using baseline levels such as UFF also capture the change in the structure-property mapping: DFT-property@DFT-geometry \rightarrow DFT-property@UFF-geometry. Training with UFF geometries circumvents computational bottlenecks in DFT-level structure optimization, for out-of-sample queries that are more expensive than Δ -SCF calculations of E_b^{1s} enabling rapid application of the ML models to new systems.

1. Atomic CM

CM is one of the simplest structure-based descriptors for mapping atomic coordinates and molecular stoichiometries to a molecular global property such as atomization energy⁵². For a molecule with N atoms, CM is an $N \times N$ matrix defined as

$$\begin{aligned} M_{ij} &= Z_i^{2.4}/2; & i = j \\ &= Z_i Z_j / R_{ij}; & i \neq j, \end{aligned} \quad (9)$$

where Z_i is the atomic number of atom- i while R_{ij} is the Euclidean distance between nuclei i and j in Å. Changing the unit of coordinates will reflect in the kernel-width, σ . The off-diagonal elements in the CM represent Coulomb interaction between the nuclei of atoms; the diagonal element is an estimation of the atomic total energy⁴⁵.

The CM is symmetric and invariant to rotation and translation but not to the choice of atomic indices. To make CM atom-index invariant, one can uniquely permute its rows and columns based on a metric⁸². The row-sorted norm version is a popular approach⁸³. The randomly sorted CM approach⁸³ considers different shuffles, included as separate training examples, offering lower prediction errors than the row sorted approach⁸⁴. As CM is symmetric, either the upper or the lower triangular matrix is sufficient to construct the descriptor vector.

In the atomic CM (ACM), each query atom, q , is represented by an $N \times N$ matrix. The indices of the N atoms are permuted in ascending order of distances of the neighboring atoms from the query atom, q . We do not apply a cut-off radius to determine the neighbor atoms. To ensure that all the entries have the same descriptor size, the size of ACM is allocated to $M \times M$ where $M = 23$ is the maximum number of atoms in the bigQM7 ω dataset cor-

responding to n -heptane. All elements of the ACM other than the $N \times N$ block are set to zero. The indexing of the atoms for ACM is schematically shown in Figure S2 of SI.

2. AtmEnv: Descriptor from Graph Neural Network

Inspired by previous research works^{41,44,85}, we have selected SchNetpack architecture (version 0.3)⁸⁶ to train a descriptor encoding the atomic environment on-the-fly^{87,88}. Some recent works^{41,44} have demonstrated the use of atomic features from trained GNN models to predict the atomic properties such as pKa, NMR shielding, and frontier MO energies for the QM9 dataset using different ML algorithms. The SchNet framework was originally developed to explore molecular potential energy surfaces, making total energy or atomization energy a suitable target for generating embeddings with the GNN. These embeddings are effective for modeling atomic forces due to the direct correlation between total energy and atomic forces. However, to model CEBEs that do not directly correlate with total energy, we have adapted the approach by training SchNet in an unsupervised manner using a null target. The descriptors so obtained from SchNetpack are referred to as ‘AtmEnv’. After unsupervised training with a null target, the SchNet model, with its optimized weights and embeddings, can be used to extract the AtmEnv vector for a query atom, employing the UFF-level molecular geometry as input. This approach enables the embeddings to be applicable for tasks beyond those directly related to total energy or forces. Using a null target (i.e., setting target values to zero) allows the embeddings to capture geometric features independent of any specific property, similar to other descriptors like SOAP, ACM, or FCHL^{89,90}.

SchNetpack belongs to the family of convolutional NN and initializes the atomic descriptors as a basis set expansion in atomic numbers, Z_i

$$y_i^{(0)} = y_i(Z_i), \quad (10)$$

where $y_i^{(0)}$ is the initial feature vector (layer = 0) for an atom, i , and $y_i(Z_i)$ are the coefficients expanded in nuclear charges, Z_i . The SchNet architecture consists of atomwise layers and convolution layers. In the atomwise layers the feature vector, y_i , for an atom i is updated as

$$y_i^{l+1} = W^l y_i^l + b^l \quad (11)$$

while in the convolution layer, y_i is updated as

$$y_i^{l+1} = \sum_j y_j^l \circ W^l(r_{ij}), \quad (12)$$

where the summation is over all the neighboring atoms of j , and the convolution operator, \circ , denotes element-wise multiplication. In both cases, y_i^{l+1} is the updated

feature vector in layer l , W^l and b^l are the network weights and bias weights, respectively, for layer, l . Further, W^l is the filter containing information about all the interatomic distances, r_{ij} , and y_j^l are the features of the neighbor atoms in layer, l . The convolutional layers in SchNet form the interaction blocks where the feature vector of one atom *interacts* with the feature vectors of other neighbors; numerous iterations lead to an updated embedding vector.

The activation function in the network is kept as shifted softplus, defined as $ssp(y) = \log[\exp(y)/2 + 1/2]$. The interatomic distances are provided in the form of Gaussian RBFs in the interaction blocks leading to learning of the AtmEnv. We used a cut-off radius of 6Å to define the neighbor atoms along with 40 Gaussian functions and 4 interaction blocks. Further, we limit the length of the AtmEnv vectors to 128, beyond which the accuracy of the KKR-ML models does not improve substantially, see Table S3.

III. RESULTS AND DISCUSSIONS

A. Assessment of DFT methods for data-generation

For the smallest 32 molecules of bigQM7 ω with 1-3 CONF atoms, excluding oxygen molecule which has a triplet ground state, we calculated E_b^{1s} using the $G_{\Delta H}W_0$ method and performed complete basis set extrapolations. Quasiparticle energies were assigned using Mulliken populations, as discussed in II B. Individual values of E_b^{1s} are provided in Table S4 of SI, which we use as the reference to assess the accuracy of E_b^{1s} determined using the mGGA functionals, TPSS and SCAN. The mGGA-DFT methods were selected due to their reduced computational complexity compared to hybrid-DFT methods, while exhibiting good accuracies for modeling KS quasi-particle energies and the bandgaps in solids^{91,92}. Furthermore, a previous study has shown that the accuracy of SCAN based Δ -SCF²⁰ can surpass that of GW methods⁶¹. The error metrics for E_b^{1s} predicted by the Δ -SCF approach (Eq. 1) and the Koopmans' approximation (Eq. 2) are tabulated in TABLE I.

For TPSS and SCAN, the error metrics are similar with their standard deviations agreeing to < 0.05 eV, suggesting either of the mGGA functionals to be appropriate for Δ -SCF estimation of E_b^{1s} . The impact of using frozen orbitals in Koopmans' approximation is apparent from the severe underestimation (>17 eV) of E_b^{1s} with the error increasing systematically with atomic number. Specifically, for SCAN/Tight-Full, the MAE is 17.73 eV for C, which increases to 19.86, 22.44, and 25.80 eV for N, O, and F, respectively. The variation between the basis sets when using the same DFT method is negligible, with NAO-VCC-5Z showing slightly lower errors when compared to Tight-Full. In some evaluatory calculations, NAO-VCC-5Z resulted in non-convergence of the density for core-ionized cations. Hence, we use Tight-Full

TABLE I. Accuracy of DFT-predicted E_b^{1s} of 32 molecules in bigQM7 ω , each containing up to three CONF atoms. DFT results were derived using Δ -SCF and Koopmans' approximations, using reference values obtained from CBS-extrapolated $G_{\Delta H}W_0$ @PBE calculations. Tight, and VCC-5Z refer to Tight-Full and NAO-VCC-5Z basis sets. The assessment includes various error metrics: mean signed error, MSE (in eV) calculated as GW -DFT, mean absolute error, MAE (in eV), and standard deviation of the error, SD (in eV).

Atom (#)	Method	DFT/Basis set	Error metrics			
			MSE	MAE	SD	
C (#49)	Δ -SCF	SCAN/Tight	-0.13	0.13	0.11	
		SCAN/VCC-5Z	-0.08	0.09	0.11	
	"	TPSS/Tight	-0.06	0.08	0.09	
		TPSS/VCC-5Z	-0.01	0.07	0.09	
	"	$-\varepsilon_{1s}$	SCAN/Tight	17.73	17.73	0.25
		"	SCAN/VCC-5Z	17.87	17.87	0.25
	"	"	TPSS/Tight	19.06	19.06	0.28
		"	TPSS/VCC-5Z	19.08	19.08	0.28
N (#12)	Δ -SCF	SCAN/Tight	-0.13	0.14	0.12	
		SCAN/VCC-5Z	-0.10	0.12	0.12	
	"	TPSS/Tight	-0.05	0.09	0.12	
		TPSS/VCC-5Z	-0.02	0.09	0.12	
	"	$-\varepsilon_{1s}$	SCAN/Tight	19.86	19.86	0.28
		"	SCAN/VCC-5Z	19.96	19.96	0.32
	"	"	TPSS/Tight	21.43	21.43	0.29
		"	TPSS/VCC-5Z	21.45	21.45	0.30
O (#11)	Δ -SCF	SCAN/Tight	-0.51	0.51	0.15	
		SCAN/VCC-5Z	-0.41	0.41	0.15	
	"	TPSS/Tight	-0.43	0.43	0.15	
		TPSS/VCC-5Z	-0.32	0.32	0.14	
	"	$-\varepsilon_{1s}$	SCAN/Tight	22.44	22.44	0.30
		"	SCAN/VCC-5Z	22.45	22.45	0.30
	"	"	TPSS/Tight	24.05	24.05	0.30
		"	TPSS/VCC-5Z	24.10	24.10	0.30
F (#8)	Δ -SCF	SCAN/Tight	-0.94	0.94	0.12	
		SCAN/VCC-5Z	-0.83	0.83	0.17	
	"	TPSS/Tight	-0.89	0.89	0.09	
		TPSS/VCC-5Z	-0.75	0.75	0.13	
	"	$-\varepsilon_{1s}$	SCAN/Tight	25.80	25.80	0.50
		"	SCAN/VCC-5Z	25.82	25.82	0.47
	"	"	TPSS/Tight	27.78	27.78	0.45
		"	TPSS/VCC-5Z	27.82	27.82	0.47

for calculating E_b^{1s} for bigQM7 ω molecules.

B. Distribution of 1s-CEBs of CONF atoms

For an atom in different molecular configurations, E_b^{1s} is influenced by a combination of the chemical environment provided by the neighboring atoms⁹ and screening effects¹⁵. Normalized distributions of E_b^{1s} for different hybridizations of the CONF atoms in bigQM7 ω are shown in FIG. 2. The distribution is heavily biased towards sp^3 -C with about thirty two thousand (32k) atoms, constituting about 38% of 85k atoms in the dataset. Conversely, sp -N is the least represented, with only 886 atoms amounting to 0.01% of the dataset. The challenge in as-

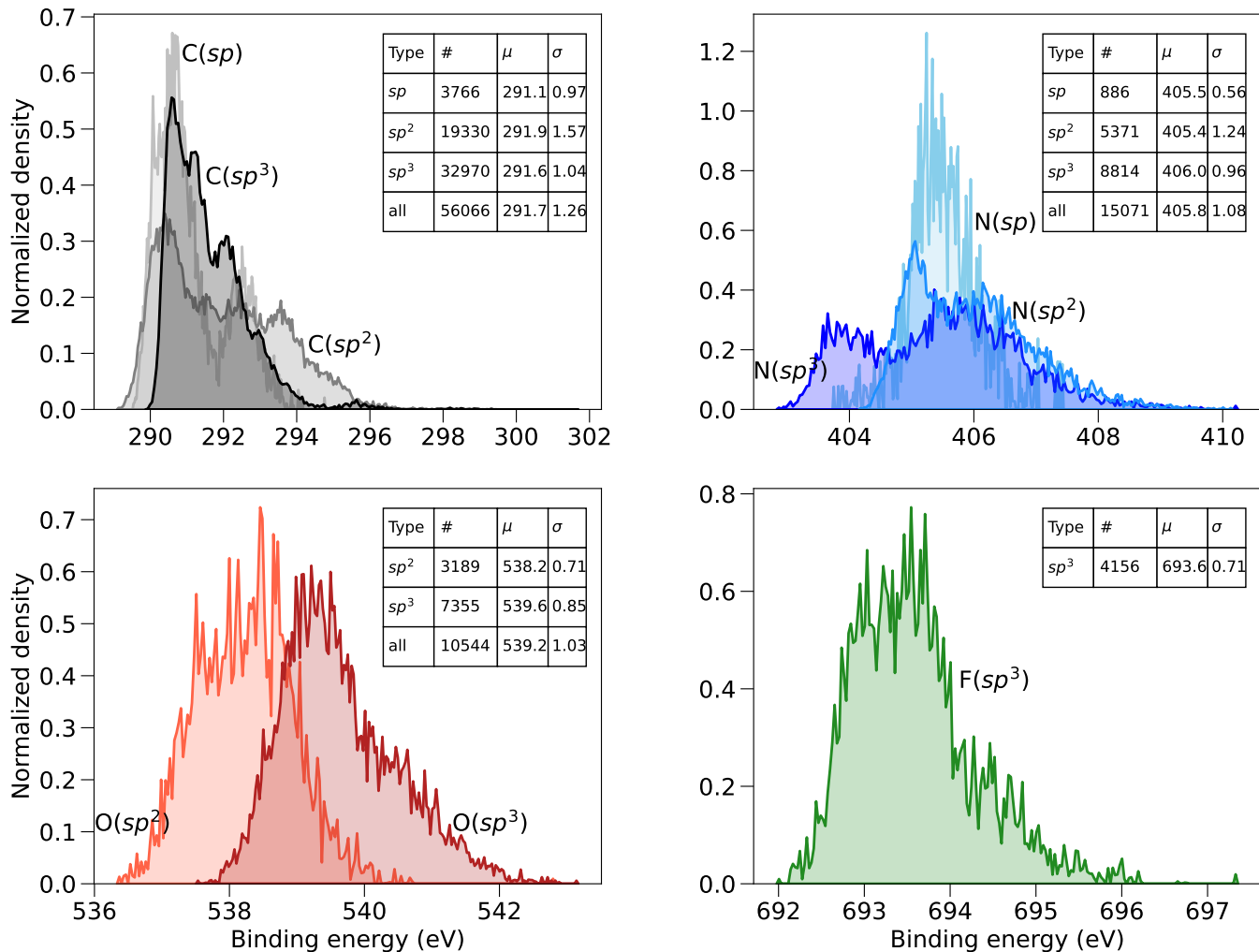


FIG. 2. Normalized density plots of CEBEs for distinct hybridizations of CONF atoms in the bigQM7 ω dataset. ‘#’ represents the number of entries, while mean, ‘ μ ’ and standard deviation, ‘ σ ’ are presented in eV.

signing E_b^{1s} lies in the fact that these energies span narrow ranges with multiple chemical environments giving rise to identical values.

In the bigQM7 ω dataset, E_b^{1s} of F and C atoms have spreads of 0.71 and 1.26 eV, respectively (see FIG. 2). Separation into individual hybridizations does not decrease the spread of distribution. In some cases, the standard deviation worsens compared to the unseparated distribution. The high compositional diversity of the bigQM7 ω dataset renders substructure classification difficult due to the several unique connectivities possible for each atom type. We analyzed a subset of bigQM7 ω comprising 24 molecules with the unique substructure: sp^2 -C bonded to N via a double bond, while bonded to O and F atoms through single bonds. See Figure S3 a) of the SI for the corresponding molecular structures. All molecules in the subset are 5-membered heterocyclic rings containing C, N, and O atoms that define the substructure. For the 25 F atoms in this molecular set, the distribution of E_b^{1s} span a range of 1.9 eV

with a standard deviation of 0.5 eV, only 0.2 eV lower than that of all 4156 F atoms in the bigQM7 ω dataset. A comparison of the distributions is shown in Figure S3 b) of the SI. This indicates that partitioning E_b^{1s} of CONF atoms in bigQM7 ω based on substructure similarity does not decrease the spread of the values, and the scope for generating separate ML models based on substructure classification is limited.

C. Optimization of ML models

We probed the impact of the length of AtmEnv descriptor vector on the accuracy of KRR-ML models of E_b^{1s} of C atoms. Results, detailed in Table S3 of the SI, show that the out-of-sample prediction accuracy improves marginally going from a length of 128 to 1024 for direct-ML predictions. Given an error of approximately 0.1 eV at length 128, the errors for lengths 32 and 64 are likely to exceed 0.1 eV. For Δ -ML, the accuracy remains

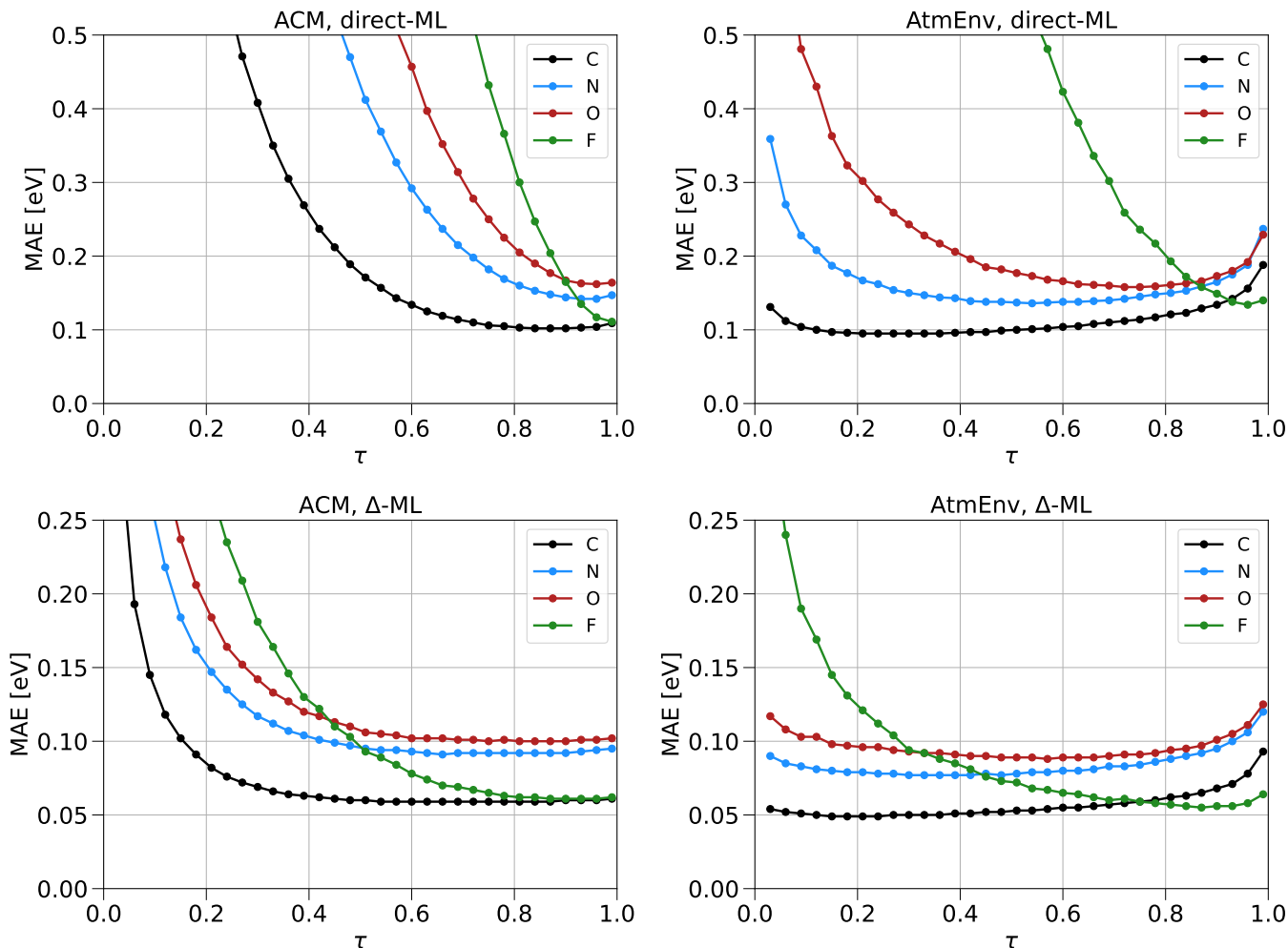


FIG. 3. Variation of MAE (in eV) with τ for estimating the kernel width (σ), see Eq. 8 in the main text. Out-of-sample errors for predicting E_b^{1s} of C/N/O/F atoms in the bigQM7 ω dataset are shown. Each point on a plot represents the out-of-sample error from an 80/20 train-test split. ACM denotes the atomic Coulomb matrix, while AtmEnv denotes the atomic environment determined from a graph neural network framework. The scheme direct-ML corresponds to learning on the target E_b^{1s} at the SCAN/Tight-Full level. For Δ -ML, the target quantity is the difference: $E_b^{\Delta-SCF}(\text{SCAN}) - E_b^{\text{Koopmans}}(\text{PBE@UFF})$; see the main text for more details. For each element, the `cebeconf` program uses τ corresponding to smallest MAE.

at 0.05 eV for length 128, slightly decreasing by only 7 meV at length 1024. Our goal of achieving an MAE below 0.1 eV for data-driven predictions of E_b^{1s} while keeping the computational complexity minimal led us to limit the length of AtmEnv to 128.

In order to visualize AtmEnv obtained from SchNet, we considered six classes of molecules not necessarily contained in bigQM7 ω : (a) $\text{CH}_3\text{-R}$, (b) $\text{CH}_3\text{-CH}_2\text{-R}$, (c) $\text{H}_2\text{C}=\text{C}(\text{H})\text{-R}$, (d) $\text{HC}\equiv\text{C-R}$, (e) substituted benzene ($\text{C}_6\text{H}_5\text{-R}$), and (f) substituted cyclohexane ($\text{C}_{12}\text{H}_{11}\text{-R}$), where $\text{R} = \text{H}, \text{CH}_3, \text{NH}_2, \text{OH}, \text{and F}$. We used a trained SchNet model to generate AtmEnv for the ‘C’ atom marked and plotted the heatmaps shown in Figure S4 of the SI. The variations in the elements of AtmEnv, associated with groups bonded to C, demonstrate how SchNet embeddings capture atomic environments. Although embeddings are not physically interpretable, they encapsu-

late atomic environments^{93,94}. For a fixed length of the AtmEnv vector, identical values for a given element of the vectors of different molecules indicate the presence of similar chemical environments in these molecules.

To determine the optimal kernel width, σ_{opt} , for KRR-ML, we varied the parameter τ between 0 and 1 and applied Eq. 8. For each atom type, we used randomly selected 80% of the data to determine the hold out error on the remaining 20%. Further, we used same indices across different ML/descriptor combinations: direct-ML/ACM, direct-ML/AtmEnv, Δ -ML/ACM, and Δ -ML/AtmEnv. FIG. 3 displays the variation in MAE with τ for all atom types. Δ -ML requires a smaller τ_{opt} (hence larger σ_{opt} as per Eq. 8) than direct-ML for all atoms. This indicates the optimal kernel function for direct-ML to be broader, sampling over more training examples. The sensitivity of MAE to τ increases from C to F atoms. While σ_{opt}

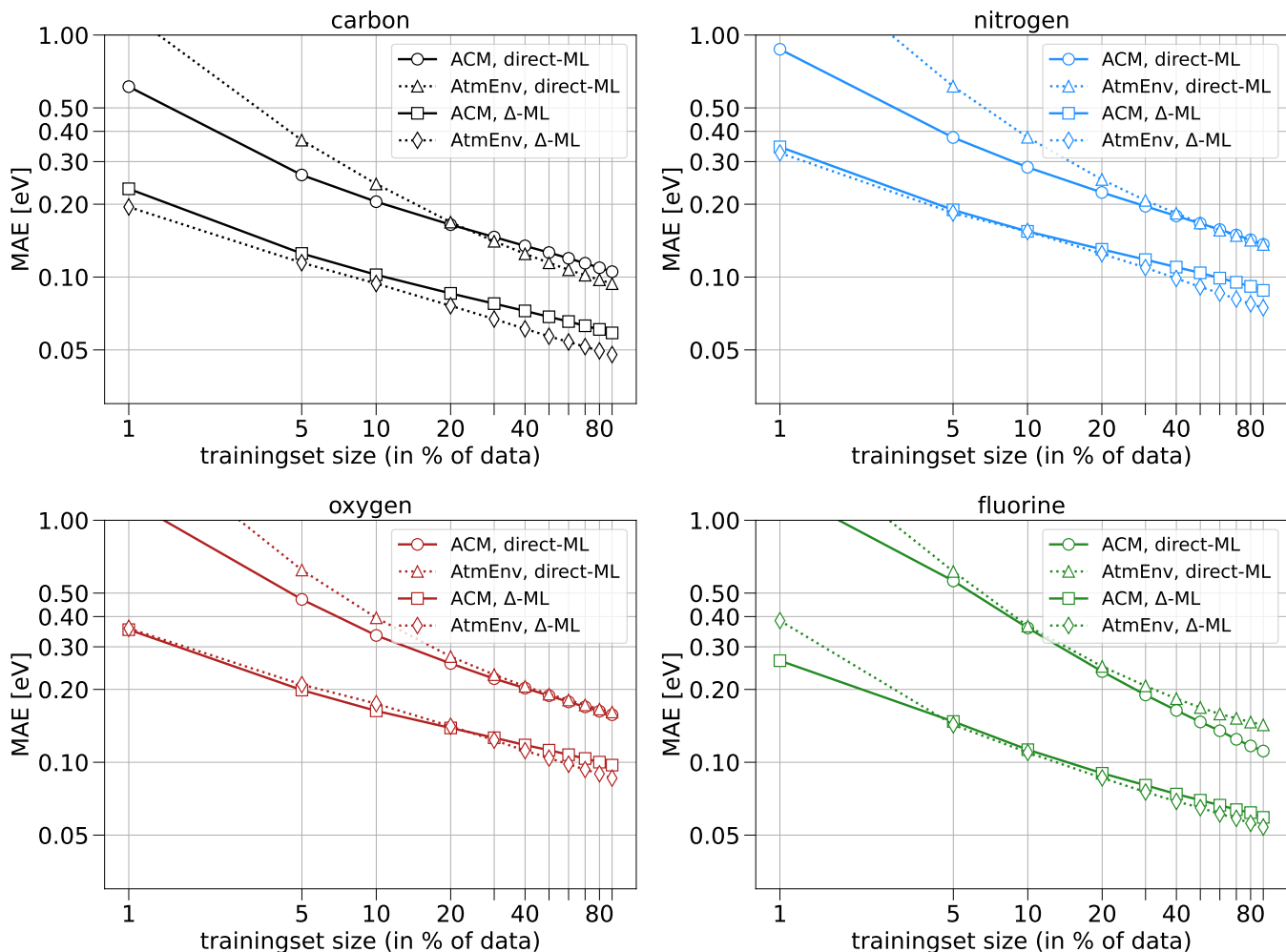


FIG. 4. Learning curves showing out-of-sample errors, as a log-log scale plot, for KRR-ML for predicting E_b^{1s} with increasing training set size. Results are shown separately for C, N, O, and F atoms. ACM and AtmEnv correspond to two variants of descriptors generated using UFF geometries. For direct-ML, the target quantity is $1s$ CEBE determined using the SCAN/Tight-Full method within the Δ -SCF formalism, while in Δ -ML, the model is trained on the difference between the target and the baseline estimation of E_b^{1s} with in the Koopmans approximation determined using the PBE/cc-pVDZ method using UFF geometries. Each curve was obtained by considering 25 data shuffles, and the mean of MAEs is plotted for various training set sizes. The standard deviation of MAEs across shuffles was negligible for large training set sizes. For clarity, we have not shown the envelope.

determined through scanning τ for E_b^{1s} -C are comparable to those determined using the heuristics proposed in a previous study⁷⁶ with $\tau = 1/2$ (see Eq. 7), precise tuning becomes crucial for modeling E_b^{1s} of F. The optimal values of σ_{opt} determined using τ corresponding to the minimum MAE in FIG. 3 and Eq. 8 are hardcoded in the trained ML models provided in the module `cebeconf`²⁹. The target accuracy (MAE < 0.1 eV) for obtaining distinct CEBEs, for resolving XPS is achieved adequately by our Δ -ML models. Figure S5 in the SI illustrates XPS predictions for a test molecule using these pre-trained models via `cebeconf`.

D. Performance of ML models for out-of-sample predictions

FIG. 4 presents learning curves depicting the MAEs for out-of-sample prediction as a function of the training set size for various KRR-ML models. The monotonous drop in MAE with the training set implies that the models capture structure-property correlation that improve with increasing example data. Overall, across CONF elements, ACM and AtmEnv show similar learning trends for direct-ML predictions. While using 90% data of E_b^{1s} -C for training in direct and Δ -ML, AtmEnv performs slightly better than ACM. Only in the case of direct-ML for E_b^{1s} -F, ACM converges to better accuracy than AtmEnv. Direct-ML predictions based on ACM and At-

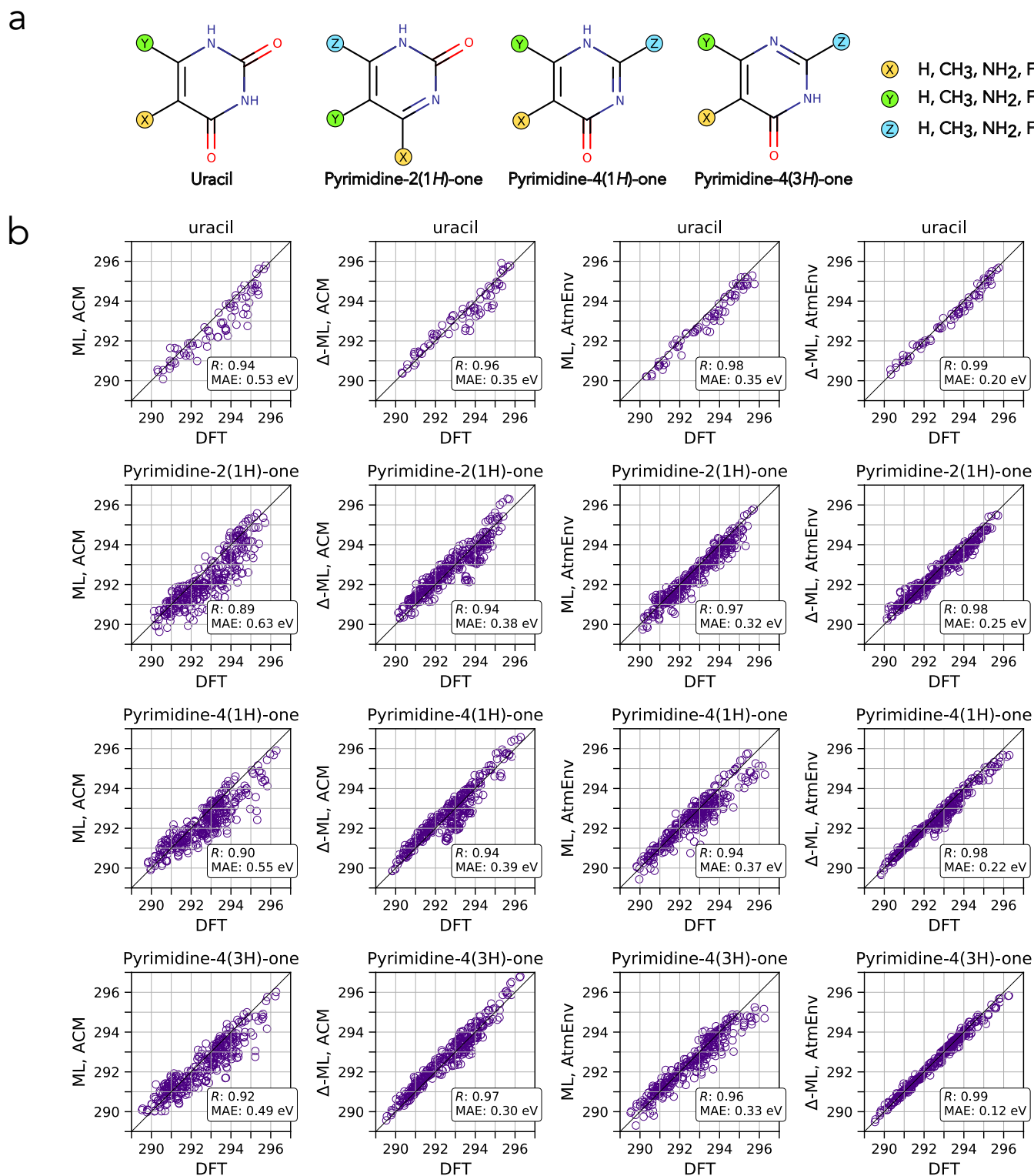


FIG. 5. a.) Combinatorially varying set of biologically relevant molecules selected for validating the E_b^{1s} predicted by the ML models presented in this study. The number of derivatives are Uracil (Pyrimidine-2,4(1H,3H)-dione): 16, Pyrimidine-2(1H)-one: 64, Pyrimidine-4(1H)-one: 64, and Pyrimidine-4(3H)-one: 64, amounting to 208 unique molecules. b.) Scatterplot comparison of ML-predicted and DFT values of E_b^{1s} -C in 208 uracil derivatives. For all four classes of molecules, ML and Δ -ML predictions are shown along with the Pearson correlation coefficient (R) and mean absolute error (MAE).

TABLE II. Prediction errors for the direct-ML and Δ -ML models of E_b^{1s} for 208 uracil-type molecules depicted in FIG. 5. Errors are quantified with reference to the target values determined at the SCAN/Tight-Full level of theory within the Δ -SCF formalism. The input for the ML models are structures determined using the universal force field (UFF). For Δ -ML, $1s$ energies of core-type molecular orbitals determined at the PBE/cc-pVDZ level using UFF geometries were used as the baseline. For a fixed ML model shared through the `cebeconf` module, prediction errors for 208 uracil-type molecules are reported as the mean absolute error (MAE) and the standard deviation of the errors (SD) in parentheses. Both MAE and SD are in eV. Pearson correlation coefficient, denoted by R , and the Spearman rank correlation coefficient, denoted by ρ , are also included. Error metrics are provided separately for carbon (C), nitrogen (N), oxygen (O), and fluorine (F) atoms within each set of molecules. The number of atoms of each type present in the set is included in the adjoining parentheses. The labels P2(1H), P4(1H), and P4(3H) correspond to Pyrimidine-2(1H)-one, Pyrimidine-4(1H)-one, and Pyrimidine-4(3H)-one, respectively.

Atom	Molecules	ML/ACM	Δ -ML/ACM	ML/AtmEnv	Δ -ML/AtmEnv
		MAE (SD), R , ρ			
C(72)	uracil	0.53 (0.53), 0.94, 0.95	0.35 (0.45), 0.96, 0.97	0.35 (0.28), 0.98, 0.98	0.20 (0.22), 0.99, 0.99
C(304)	P2(1H)	0.63 (0.64), 0.89, 0.90	0.38 (0.48), 0.94, 0.94	0.32 (0.35), 0.97, 0.97	0.25 (0.30), 0.98, 0.98
C(304)	P4(1H)	0.55 (0.61), 0.90, 0.90	0.39 (0.48), 0.94, 0.92	0.37 (0.47), 0.94, 0.93	0.22 (0.26), 0.98, 0.98
C(304)	P4(3H)	0.49 (0.58), 0.92, 0.92	0.30 (0.33), 0.97, 0.97	0.33 (0.43), 0.96, 0.96	0.12 (0.17), 0.99, 0.99
N(40)	uracil	0.39 (0.28), 0.81, 0.73	0.22 (0.16), 0.96, 0.96	0.48 (0.38), 0.74, 0.80	0.23 (0.23), 0.92, 0.90
N(176)	P2(1H)	0.45 (0.56), 0.90, 0.89	0.19 (0.22), 0.98, 0.98	0.47 (0.45), 0.93, 0.88	0.16 (0.20), 0.99, 0.99
N(176)	P4(1H)	0.46 (0.49), 0.95, 0.96	0.20 (0.25), 0.99, 0.99	0.57 (0.58), 0.89, 0.84	0.22 (0.28), 0.99, 0.99
N(176)	P4(3H)	0.39 (0.41), 0.90, 0.90	0.18 (0.20), 0.98, 0.98	0.76 (0.59), 0.84, 0.82	0.13 (0.16), 0.99, 0.99
O(32)	uracil	0.32 (0.33), 0.73, 0.73	0.21 (0.22), 0.95, 0.94	0.26 (0.24), 0.77, 0.74	0.09 (0.10), 0.96, 0.96
O(64)	P2(1H)	0.22 (0.30), 0.82, 0.82	0.24 (0.22), 0.94, 0.94	0.51 (0.45), 0.16, 0.12	0.15 (0.18), 0.89, 0.87
O(64)	P4(1H)	0.28 (0.25), 0.82, 0.79	0.33 (0.18), 0.96, 0.96	0.49 (0.34), 0.68, 0.66	0.25 (0.13), 0.94, 0.94
O(64)	P4(3H)	0.30 (0.38), 0.61, 0.56	0.20 (0.16), 0.96, 0.95	0.29 (0.31), 0.73, 0.71	0.08 (0.09), 0.98, 0.98
F(8)	uracil	0.40 (0.16), 0.97, 0.98	0.07 (0.07), 0.99, 1.00	0.47 (0.28), 0.95, 0.95	0.15 (0.14), 0.96, 1.00
F(48)	P2(1H)	0.35 (0.37), 0.72, 0.69	0.20 (0.09), 0.99, 0.98	0.40 (0.41), 0.79, 0.79	0.14 (0.16), 0.96, 0.97
F(48)	P4(1H)	0.25 (0.30), 0.83, 0.82	0.20 (0.12), 0.97, 0.98	0.45 (0.50), 0.62, 0.59	0.18 (0.19), 0.93, 0.93
F(48)	P4(3H)	0.32 (0.38), 0.71, 0.68	0.17 (0.12), 0.98, 0.98	0.53 (0.63), 0.10, 0.08	0.22 (0.21), 0.93, 0.93

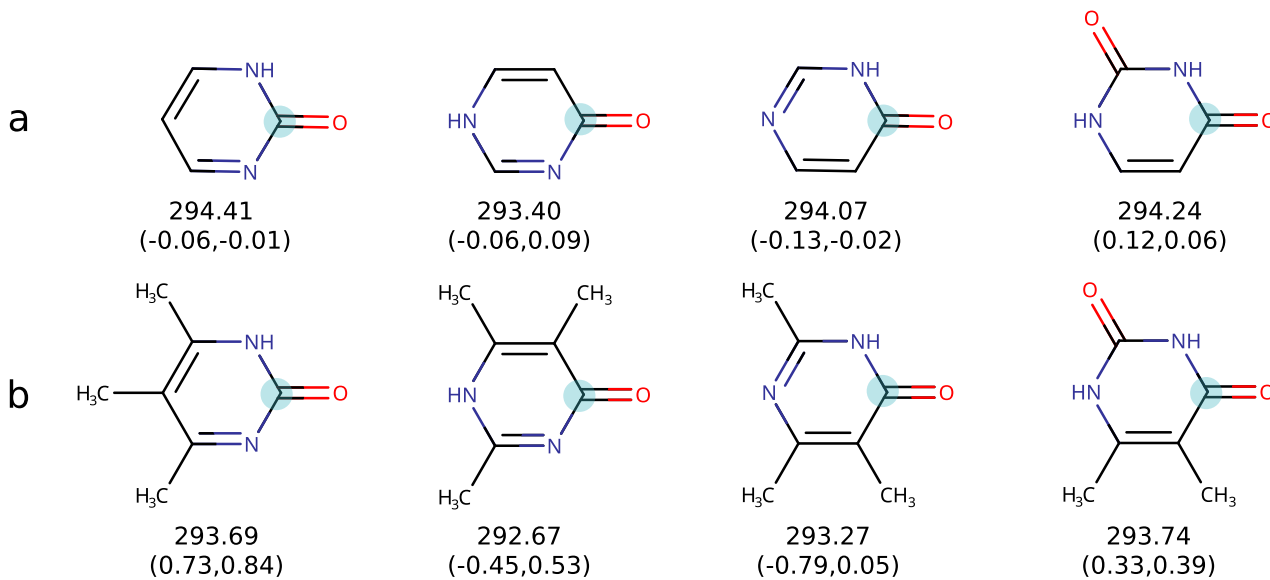


FIG. 6. Effect of substitution of methyl groups ($-\text{CH}_3$) in the base molecules, shown in row-a, on the E_b^{1s} -C of the carbonyl group (blue circle). See the caption of FIG. 5a for the names of the molecules. Corresponding methylated molecules are shown in row-b. SCAN/Tight-Full, Δ -SCF-based E_b^{1s} (in eV) of the C atom are given below each molecule. Error in predictions of direct-ML/AtmEnv and Δ -ML/AtmEnv with respect to Δ -SCF values are given in parenthesis.

mEnv offer similar accuracies for N and O. In Δ -ML, AtmEnv delivers consistently lower MAE compared to ACM for modeling 1s-CEBEs of all elements.

As discussed in III B, E_b^{1s} of C is the most represented consisting of $\approx 65\%$ of the bigQM7 ω -CEBECONF dataset, achieving Δ -ML MAE of 0.05 eV with AtmEnv descriptor. Additionally, the MAE for E_b^{1s} -F when using the $\geq 80\%$ of the data for training drops below 0.07 eV. However, a look at the distribution and composition of the F set offers insight into this high accuracy. Apart from the possibility of a single hybridization, all F atoms are connected to sp^3 C atoms, except the outliers HF and F₂, making the set compositionally more uniform compared to N and O. Hence, the distribution of E_b^{1s} -F also has a lower standard deviation compared to C/O/N, see 2. While N and O groups have a higher compositional diversity compared to F, their training sizes are not large compared to C, resulting in higher MAEs. Overall, for data-driven predictions of E_b^{1s} of C/O/N/F atoms to an accuracy of ≤ 0.1 eV, Δ -ML approach is necessary; the target accuracy is reached with 10%, 40%, 60%, and 20% of the data for C, N, O, and F atoms, respectively. Decreasing the error further may require better baselines in Δ -ML or better geometries, both may incur additional expenses for out-of-sample predictions.

E. Transferability Test for ML models

Since E_b^{1s} is a property of an atom in a molecule, it is of interest to explore the transferability of the ML models trained on bigQM7 ω to new class of molecules. Hence, we have selected a set of aromatic heterocyclic systems as a validation set. Its composition is motivated by the potential application of the ML-models of E_b^{1s} to identify the composition of small biomolecules such as derivatives of nucleic acid bases, heavily substituted by O and N. Additionally, the use of substituted pyrimidines for synthesis is common⁹⁵. Particularly, up to two carbonyl groups have been included in pyrimidines generating derivatives of uracil, pyrimidine-2(1H)-one, pyrimidine-4(1H)-one and pyrimidine-4(3H)-one, see FIG. 5a. C atoms not attached to carbonyls are combinatorially substituted with either H, CH₃, NH₂ or F.

Each of the three pyrimidinones has a carbonyl group and three sites for substitution, leading to 64 derivatives in each class, summing to 192 molecules. Additionally, 16 substituted uracils are generated, since there are 2 carbonyls attached to a pyrimidine, availing the remaining 2 C atoms for substitution. These molecules contain 7-10 CONF atoms. The number of molecules containing 7,8,9 and 10, CONF atoms, are 1, 9, 27 and 27, respectively in each of the pyrimidinone sets. The uracil set has 1,6 and 9, molecules with 8,9, and 10 CONF atoms, respectively. Together, these 208 molecules constitute our validation set. Among them, only one (unsubstituted pyrimidine-2(1H)-one) is contained in bigQM7 ω . Along with this molecule, pyrimidine-4(1H)-one and pyrimidine-4(3H)-

one are the only molecules in the validation set with 7 heavy atoms, while the remaining 206 molecules are composed of more than 7 CONF atoms. Baseline energies for Δ -ML are obtained at the same level of theory as in the training set, with aZORA corrected KS-eigenvalues obtained with the PBE/cc-pVDZ method using UFF-level molecular structures. One can also use the non-relativistic variant of these energies and correct them by adding 0.29/0.55/0.97/1.57 eV for C/O/N/F atoms, respectively as stated in Figure S1.

ML-predicted CEBEs alongside DFT values are represented in scatter plots for all the ML models featured in FIG. 5b. Corresponding atom-specific errors for each class of molecules are tabulated in TABLE II. Alike out-of-sample predictions in bigQM7 ω , discussed in III D, the performance of direct-ML is inferior to that of Δ -ML. In general, a correlation coefficient above 0.7 is considered to indicate a strong linear correlation in different disciplines^{96,97}. In this study, all Δ -ML models achieve a high Pearson’s correlation coefficient, $R \approx 0.9$, for all classes of validation molecules, as shown in FIG. 5 and TABLE II. Similarly, all direct-ML models exhibit correlation coefficients of $\gtrsim 0.7$, with the exception of two cases where the correlation is weak. ACM models perform slightly worse, with direct-ML models based on ACM performing the poorest of all models, Δ -ML/ACM has performance similar to direct-ML/AtmEnv predictions. Δ -ML with AtmEnv shows the least errors, with $R \geq 0.98$. In terms of element-specific accuracy, ACM has better prediction for N and F systems. Compared to explorations with the bigQM7 ω dataset, the accuracy of ML models has somewhat deteriorated while applying to large biomolecules. This is due to the fact that the molecules in the validation set are larger than those used for training the models. However, the qualitative trends between E_b^{1s} and the structural variations is captured by our ML models, indicated by the high correlation coefficients.

In FIG. 6, we compare ML-predicted E_b^{1s} with that of DFT values for the four unsubstituted bases shown in FIG. 5a and their CH₃ substituted counterpart shown in FIG. 5b. In particular, we explore the CEBEs of the C atom in a carbonyl group common to all four base molecules. Both direct- and Δ -ML predictions show excellent accuracy for unsubstituted pyrimidine-2(1H)-one, which is contained in the bigQM7 ω dataset. For all four unsubstituted molecules, the Δ -ML predictions show an error of < 0.1 eV. Upon methylation, the CEBE at the carbonyl C decreases according to DFT predictions, while there is a drastic depreciation in the prediction accuracy of ML models. All predictions for the substituted molecules have errors above 0.3 eV except a single case of Δ -ML prediction, where the prediction is within an error of 0.05 eV. The same C with direct ML doesn’t show a similar drop in error, even though the training data is same for both direct-ML and Δ -ML. Overall, this test of transferability of Δ -ML/AtmEnv based on an inexpensive baseline suggests that CEBEs can be assigned to

class of molecules with systematic variation of structure and composition with high degree of linear correlation. However, the models do not offer quantitative accuracy for the prediction of E_b^{1s} when the application is limited to a few molecules, as the models based on local descriptors do not capture long-range stereo-electronic effects resulting in accumulation of systematic errors.

IV. CONCLUSION

In this study, we showcased the applicability of ML models for prediction of XPS. Using CEBEs determined using Δ -SCF calculations, we generated the database, bigQM7 ω -CEBECONF, consisting of 12679 molecules from the bigQM7 ω dataset amounting to 85837 1s-CEBE of CONF atoms. For ML modeling, we explored the use of two descriptors: ACM, a local version of Coulomb matrix, and AtmEnv, a representation obtained from atom-specific embeddings of a graph neural network framework. KRR models were optimized by tuning the kernel widths determined specifically for each atomic model. The ML models reported in this study bypass the use of many body calculations or charge constraining algorithms, using only structural description of the molecule for predicting CEBEs. These models have been made accessible for general use through the python module `cebeconf`²⁹, where UFF level structures can be given as input to get CEBEs. The accuracy is leveraged further with the use of Δ -ML using inexpensive baseline KS eigenvalues from single-point calculation on molecular geometry determined with force-fields.

For out-of-sample predictions within the bigQM7 ω dataset, Δ -ML in combination with the AtmEnv descriptor offers an accuracy of less than 0.1 eV, which is an order of magnitude smaller than the spread of 1s-CEBE in the bigQM7 ω dataset. To understand the transferability of the models, we applied them to 208 biomolecules with homogeneously varying structure and compositions. Since these molecules are larger than the bigQM7 ω molecules used for training, their accuracy dropped compared to out-of-sample predictions within the bigQM7 ω dataset. However, they yield an overall correlation coefficient of over 0.9, underscoring the crucial role of correlation in indicating that the prediction errors are largely systematic. This high correlation coefficient suggests that the model may be suitable for large-scale predictions, as it can be effectively calibrated using a few CEBEs determined at the target level.

This study extends the applicability of currently available ML models for XPS prediction to organic molecules. Such models of quasi-atomic properties can be extended to atoms beyond CONF, such as alkali and alkaline elements⁹⁸, transition metal atoms⁹⁹, and others¹⁰⁰. Currently, large datasets needed for ML modeling for other elements are lacking. Experimental references¹⁰¹ can serve as a starting point for selecting computational

chemistry methods that can be employed for data generation.

V. SUPPLEMENTARY MATERIAL

See the supplementary material for the following: Figure S1 shows linear fits to obtain aZORA corrections for non-relativistic baseline energies. Figure S2 presents the choice of atomic indices in ACM representation on a schematic molecule. Figure S3 displays structures and normalized density plots for molecules with an identical substructure. Figure S4 shows the heatmaps of AtmEnv of ‘C’ atom in six classes of molecules. Figure S5 shows the use of `cebeconf`. Table S1 shows the splitting of CEBEs in benzene. Table S2 gives the composition of the bigQM7 ω -CEBECONF dataset. Table S3 shows the variation of MAE for direct-ML and Δ -ML with the length of AtmEnv. Table S4 provides the $G_{\Delta H}W_0$ energies at cc-pVnZ and extrapolated values at CBS limit. Table S5 Table S5 provides statistics of molecules exhibiting convergence failure. Table S6 gives the list of SMILES of molecules exhibiting convergence failure. The trained ML models are provided along with example validations at <https://github.com/moldis-group/cebeconf>²⁹.

VI. DATA AVAILABILITY

The data that support the findings of this study are within the article and its supplementary material.

VII. ACKNOWLEDGMENTS

We thank Miguel Caro for providing the geometries of a subset of QM9 used in Ref. 38. We thank Stijn De Baerdemacker for sharing the preprint of Ref. 41. ST thanks Dorothea Golze for commenting on questions regarding *GW* calculations. We thank Atreyee Majumder for assistance in calculations. We acknowledge the support of the Department of Atomic Energy, Government of India, under Project Identification No. RTI 4007. All calculations have been performed using the Helios computer cluster, which is an integral part of the MolDis Big Data facility, TIFR Hyderabad (<http://moldis.tifrh.res.in>).

VIII. AUTHOR DECLARATIONS

A. Author contributions

ST: Conceptualization (equal); Analysis (equal); Data collection (main); Writing (equal). **SD**: Analysis (equal); Writing (equal). **SJ**: Analysis (equal); Writing (equal). **RR**: Conceptualization (equal); Analysis (equal); Funding acquisition; Project administration and supervision; Resources; Writing (equal).

B. Conflicts of Interest

The authors have no conflicts of interest to disclose.

REFERENCES

- ¹F. de Groot and A. Kotani, *Core Level Spectroscopy of Solids* (CRC Press, 2008).
- ²P. S. Bagus, C. Sousa, and F. Illas, *J. Phys.: Condens. Matter* **34**, 154004 (2022).
- ³K. Diller, F. Klappenberger, F. Allegretti, A. C. Papageorgiou, S. Fischer, D. A. Duncan, R. J. Maurer, J. A. Lloyd, S. C. Oh, K. Reuter, and J. V. Barth, *J. Chem. Phys.* **141**, 144703 (2014).
- ⁴M. Ayiania, M. Smith, A. J. Hensley, L. Scudiero, J.-S. McEwen, and M. Garcia-Perez, *Carbon* **162**, 528 (2020).
- ⁵W. Feng, H. Zhou, and S.-z. Yang, *Mater. Chem. Phys.* **124**, 287 (2010).
- ⁶P. Willmott, *An introduction to synchrotron radiation: techniques and applications* (John Wiley & Sons, 2019).
- ⁷B. Kovač, I. Ljubić, A. Kivimäki, M. Coreno, and I. Novak, *Phys. Chem. Chem. Phys.* **16**, 10734 (2014).
- ⁸G. Azuara-Tuexi, E. Muñoz-Sandoval, and R. Guirado-López, *Phys. Chem. Chem. Phys.* **25**, 3718 (2023).
- ⁹G. Greczynski and L. Hultman, *Prog. Mater. Sci.* **107**, 100591 (2020).
- ¹⁰Q. T. Trinh, K. Bhola, P. N. Amaniampong, F. Jerome, and S. H. Mushrif, *J. Phys. Chem. C* **122**, 22397 (2018).
- ¹¹L. Nguyen, F. F. Tao, Y. Tang, J. Dou, and X.-J. Bao, *Chem. Rev.* **119**, 6822 (2019).
- ¹²W. Yu, Z. Yu, Y. Cui, and Z. Bao, *ACS Energy Lett.* **7**, 3270 (2022).
- ¹³S. Kohiki, *Spectrochim. Acta Part B At. Spectrosc.* **54**, 123 (1999).
- ¹⁴D. P. Chong, O. V. Gritsenko, and E. J. Baerends, *J. Chem. Phys.* **116**, 1760 (2002).
- ¹⁵P. S. Bagus, E. S. Iltou, and C. J. Nelin, *Surf. Sci. Rep.* **68**, 273 (2013).
- ¹⁶N. A. Besley, *WIREs Comput. Mol. Sci.* **11**, e1527 (2021).
- ¹⁷F. Aryasetiawan and O. Gunnarsson, *Rep. Prog. Phys.* **61**, 237 (1998).
- ¹⁸X. Ren, P. Rinke, C. Joas, and M. Scheffler, *J. Mater. Sci.* **47**, 7447 (2012).
- ¹⁹A. R. Williams, R. A. DeGroot, and C. B. Sommers, *J. Chem. Phys.* **63**, 628 (1975).
- ²⁰S. Jana and J. M. Herbert, *J. Chem. Phys.* **158** (2023).
- ²¹P. S. Bagus, *Phys. Rev.* **139**, A619 (1965).
- ²²J. M. Kahk and J. Lischner, *Phys. Rev. Mater.* **3**, 100801 (2019).
- ²³N. Pueyo Bellafont, F. Viñes, and F. Illas, *J. Chem. Theory Comput.* **12**, 324 (2016).
- ²⁴A. T. B. Gilbert, N. A. Besley, and P. M. W. Gill, *J. Phys. Chem. A* **112**, 13164 (2008).
- ²⁵K. Carter-Fenk and J. M. Herbert, *J. Chem. Theory Comput.* **16**, 5067 (2020).
- ²⁶B. P. Klein, S. J. Hall, and R. J. Maurer, *J. Phys.: Condens. Matter* **33**, 154005 (2021).
- ²⁷J. Behler, B. Delley, K. Reuter, and M. Scheffler, *Phys. Rev. B* **75**, 115409 (2007).
- ²⁸G. S. Michelitsch and K. Reuter, *J. Chem. Phys.* **150**, 074104 (2019).
- ²⁹S. Tripathy, S. Das, S. Jindal, and R. Ramakrishnan, "cebeconf: A package of machine-learning models for predicting 1s-core electron binding energies of conf atoms in organic molecules." (2024).
- ³⁰S. Dorey, F. Gaston, S. R. Marque, B. Bortolotti, and N. Dupuy, *Appl. Surf. Sci.* **427**, 966 (2018).
- ³¹A. M. Ferraria, J. D. L. da Silva, and A. M. B. do Rego, *Polymer* **44**, 7241 (2003).
- ³²R. Ramakrishnan, P. O. Dral, M. Rupp, and O. A. Von Lilienfeld, *Sci. Data* **1**, 1 (2014).
- ³³P. Kayastha, S. Chakraborty, and R. Ramakrishnan, *Digit. Discov.* **1**, 689 (2022).
- ³⁴M. Rupp, R. Ramakrishnan, and O. A. Von Lilienfeld, *J. Phys. Chem. Lett.* **6**, 3309 (2015).
- ³⁵R. Ramakrishnan, P. O. Dral, M. Rupp, and O. A. Von Lilienfeld, *J. Chem. Theory Comput.* **11**, 2087 (2015).
- ³⁶A. Gupta, S. Chakraborty, and R. Ramakrishnan, *Mach. learn.: sci. technol.* **2**, 035010 (2021).
- ³⁷L. Watson, T. Pope, R. M. Jay, A. Banerjee, P. Wernet, and T. J. Penfold, *Struct. Dyn.* **10**, 064101 (2023).
- ³⁸D. Golze, M. Hirvensalo, P. Hernández-León, A. Aarva, J. Etula, T. Susi, P. Rinke, T. Laurila, and M. A. Caro, *Chem. Mater.* **34**, 6240 (2022).
- ³⁹T. Shiota, K. Ishihara, and W. Mizukami, *Digit. Discov.* (2024).
- ⁴⁰A. M. El-Samman, S. De Castro, B. Morton, and S. De Baerdemacker, *Can. J. Chem.* **102**, 275 (2024).
- ⁴¹A. M. El-Samman, I. A. Husain, M. Huynh, S. De Castro, B. Morton, and S. De Baerdemacker, *Digit. Discov.* **3**, 544 (2024).
- ⁴²R. Ramakrishnan, M. Hartmann, E. Tapavicza, and O. A. Von Lilienfeld, *J. Chem. Phys.* **143** (2015).
- ⁴³A. Gupta, S. Chakraborty, D. Ghosh, and R. Ramakrishnan, *J. Chem. Phys.* **155** (2021).
- ⁴⁴A. Fediai, P. Reiser, J. E. O. Peña, W. Wenzel, and P. Friederich, *Mach. learn.: sci. technol.* **4**, 035045 (2023).
- ⁴⁵R. Ramakrishnan and O. A. von Lilienfeld, *Rev. Comput. Chem.* **30**, 225 (2017).
- ⁴⁶A. Kotobi, K. Singh, D. Hö"che, S. Bari, R. H. Meißner, and A. Bande, *J. Am. Chem. Soc.* **145**, 22584 (2023).
- ⁴⁷A. Choudhury, R. Ramakrishnan, and D. Ghosh, *Chem. Commun.* (2024).
- ⁴⁸A. Aarva, V. L. Deringer, S. Sainio, T. Laurila, and M. A. Caro, *Chem. Mater.* **31**, 9243 (2019).
- ⁴⁹T. Zarrouk, R. Ibragimova, A. P. Bartók, and M. A. Caro, *J. Am. Chem. Soc.* (2024).
- ⁵⁰J.-D. Chai and M. Head-Gordon, *Phys. Chem. Chem. Phys.* **10**, 6615 (2008).
- ⁵¹A. K. Rappé, C. J. Casewit, K. Colwell, W. A. Goddard III, and W. M. Skiff, *J. Am. Chem. Soc.* **114**, 10024 (1992).
- ⁵²M. Rupp, A. Tkatchenko, K.-R. Müller, and O. A. von Lilienfeld, *Phys. Rev. Lett.* **108**, 058301 (2012).
- ⁵³V. Blum, R. Gehrke, F. Hanke, P. Havu, V. Havu, X. Ren, K. Reuter, and M. Scheffler, *Comput. Phys. Comm.* **180**, 2175 (2009).
- ⁵⁴A. Majumdar and R. Ramakrishnan, *Phys. Chem. Chem. Phys.* **26**, 14505 (2024).
- ⁵⁵S. Senthil, S. Chakraborty, and R. Ramakrishnan, *Chem. Sci.* **12**, 5566 (2021).
- ⁵⁶I. Y. Zhang, X. Ren, P. Rinke, V. Blum, and M. Scheffler, *New J. Phys.* **15**, 123033 (2013).
- ⁵⁷R. Sarangi, M. L. Vidal, S. Coriani, and A. I. Krylov, *Mol. Phys.* **118**, e1769872 (2020).
- ⁵⁸R. S. Mulliken, *J. Chem. Phys.* **23**, 1833 (1955).
- ⁵⁹N. M. O'Boyle, M. Banck, C. A. James, C. Morley, T. Vandermeersch, and G. R. Hutchison, *J. Cheminform* **3**, 1 (2011).
- ⁶⁰N. P. Bellafont, P. S. Bagus, and F. Illas, *J. Chem. Phys.* **142** (2015).
- ⁶¹J. Li, Y. Jin, P. Rinke, W. Yang, and D. Golze, *J. Chem. Theory Comput.* **18**, 7570 (2022).
- ⁶²D. Golze, J. Wilhelm, M. J. van Setten, and P. Rinke, *J. Chem. Theory Comput.* **14**, 4856 (2018).
- ⁶³D. Golze, M. Dvorak, and P. Rinke, *Front. Chem.* **7**, 377 (2019).
- ⁶⁴D. Golze, L. Keller, and P. Rinke, *J. Phys. Chem. Lett.* **11**, 1840 (2020).
- ⁶⁵D. Mejia-Rodriguez, A. Kunitsa, E. Aprà, and N. Govind, *J. Chem. Theory Comput.* **18**, 4919 (2022).
- ⁶⁶M. J. Frisch, G. W. Trucks, H. B. Schlegel, G. E. Scuseria, M. A. Robb, J. R. Cheeseman, G. Scalmani, V. Barone, G. A. Peters-

- son, H. Nakatsuji, X. Li, M. Caricato, A. V. Marenich, J. Bloino, B. G. Janesko, R. Gomperts, B. Mennucci, H. P. Hratchian, J. V. Ortiz, A. F. Izmaylov, J. L. Sonnenberg, D. Williams-Young, F. Ding, F. Lipparini, F. Egidi, J. Goings, B. Peng, A. Petrone, T. Henderson, D. Ranasinghe, V. G. Zakrzewski, J. Gao, N. Rega, G. Zheng, W. Liang, M. Hada, M. Ehara, K. Toyota, R. Fukuda, J. Hasegawa, M. Ishida, T. Nakajima, Y. Honda, O. Kitao, H. Nakai, T. Vreven, K. Throssell, J. A. Montgomery, Jr., J. E. Peralta, F. Ogliaro, M. J. Bearpark, J. J. Heyd, E. N. Brothers, K. N. Kudin, V. N. Staroverov, T. A. Keith, R. Kobayashi, J. Normand, K. Raghavachari, A. P. Rendell, J. C. Burant, S. S. Iyengar, J. Tomasi, M. Cossi, J. M. Millam, M. Klene, C. Adamo, R. Cammi, J. W. Ochterski, R. L. Martin, K. Morokuma, O. Farkas, J. B. Foresman, and D. J. Fox, "Gaussian[®] 16 Revision C.01," (2016).
- ⁶⁷E. van Lenthe, J. G. Snijders, and E. J. Baerends, *J. Chem. Phys.* **105**, 6505 (1996).
- ⁶⁸L. Keller, V. Blum, P. Rinke, and D. Golze, *J. Chem. Phys.* **153**, 114110 (2020).
- ⁶⁹B. Kempgens, H. Köppel, A. Kivimäki, M. Neeb, L. Cederbaum, and A. Bradshaw, *Phys. Rev. Lett.* **79**, 3617 (1997).
- ⁷⁰V. Myrseth, K. Børve, K. Wiesner, M. Bässler, S. Svensson, and L. Sæthre, *Phys. Chem. Chem. Phys.* **4**, 5937 (2002).
- ⁷¹U. Hergenhahn, O. Kugeler, A. Rüdél, E. E. Rennie, and A. M. Bradshaw, *J. Phys. Chem. A* **105**, 5704 (2001).
- ⁷²F. Matz, J. Nijssen, and T.-C. Jagau, *J. Phys. Chem. A* **127**, 6147 (2023).
- ⁷³K. Hansen, F. Biegler, R. Ramakrishnan, W. Pronobis, O. A. Von Lilienfeld, K.-R. Müller, and A. Tkatchenko, *J. Phys. Chem. Lett.* **6**, 2326 (2015).
- ⁷⁴A. Stuke, M. Todorović, M. Rupp, C. Kunkel, K. Ghosh, L. Himanen, and P. Rinke, *J. Chem. Phys.* **150** (2019).
- ⁷⁵B. Schölkopf, A. J. Smola, F. Bach, *et al.*, *Learning with kernel machines, regularization, optimization, and beyond* (MIT press, 2002).
- ⁷⁶R. Ramakrishnan and O. A. von Lilienfeld, *Chimia* **69**, 182 (2015).
- ⁷⁷J. Behler and M. Parrinello, *Phys. Rev. Lett.* **98**, 146401 (2007).
- ⁷⁸W. J. Szlachta, A. P. Bartók, and G. Csányi, *Phys. Rev. B* **90**, 104108 (2014).
- ⁷⁹O. T. Unke and M. Meuwly, *J. Chem. Phys.* **148** (2018).
- ⁸⁰B. Huang and O. A. von Lilienfeld, **12**, 945 (2020).
- ⁸¹F. A. Faber, A. S. Christensen, B. Huang, and O. A. Von Lilienfeld, *J. Chem. Phys.* **148** (2018).
- ⁸²O. A. Von Lilienfeld, *Int. J. Quantum Chem.* **113**, 1676 (2013).
- ⁸³G. Montavon, K. Hansen, S. Fazli, M. Rupp, F. Biegler, A. Ziehe, A. Tkatchenko, A. Lilienfeld, and K.-R. Müller, *Adv. Neural Inf. Process. Syst.* **25** (2012).
- ⁸⁴K. Hansen, G. Montavon, F. Biegler, S. Fazli, M. Rupp, M. Scheffler, O. A. Von Lilienfeld, A. Tkatchenko, and K.-R. Müller, *J. Chem. Theory Comput.* **9**, 3404 (2013).
- ⁸⁵S. Jindal, P.-J. Hsu, H. T. Phan, P.-K. Tsou, and J.-L. Kuo, *Phys. Chem. Chem. Phys.* **24**, 27263 (2022).
- ⁸⁶K. Schütt, P. Kessel, M. Gastegger, K. Nicoli, A. Tkatchenko, and K.-R. Müller, *J. Chem. Theory Comput.* **15**, 448 (2018).
- ⁸⁷H. Cho and I. S. Choi, *ChemMedChem* **14**, 1604 (2019).
- ⁸⁸G. Te, W. Hu, A. Zheng, and Z. Guo, in *Proceedings of the 26th ACM international conference on Multimedia* (2018) pp. 746–754.
- ⁸⁹Y. Mo, L. Peng, J. Xu, X. Shi, and X. Zhu, in *Proceedings of the AAAI Conference on Artificial Intelligence*, Vol. 36 (2022) pp. 7797–7805.
- ⁹⁰W. L. Hamilton, R. Ying, and J. Leskovec, arXiv preprint arXiv:1709.05584 (2017).
- ⁹¹P. Kovács, P. Blaha, and G. K. Madsen, *J. Chem. Phys.* **159** (2023).
- ⁹²R. Ramakrishnan and S. Jain, *J. Chem. Phys.* **159** (2023).
- ⁹³Z. Hu, Y. Guo, Z. Liu, D. Shi, Y. Li, Y. Hu, M. Bu, K. Luo, J. He, C. Wang, *et al.*, *J. Chem. Inf. Model.* **63**, 1756 (2023).
- ⁹⁴R. Dybowski, *New J. Chem.* **44**, 20914 (2020).
- ⁹⁵W. B. Parker, *Chem. Rev.* **109**, 2880 (2009).
- ⁹⁶B. Ratner, *J. Targeting, Meas. Anal. Marketing* **17**, 139 (2009).
- ⁹⁷H. Akoglu, *Turk J Emerg Med.* **18**, 91 (2018).
- ⁹⁸J. M. Kahk and J. Lischner, *J. Chem. Theory Comput.* **19**, 3276 (2023).
- ⁹⁹J. V. Jorstad, T. Xie, and C. M. Morales, *Int. J. Quantum Chem.* **122**, e26881 (2022).
- ¹⁰⁰K. Hirao, H.-S. Bae, J.-W. Song, and B. Chan, *J. Phys. Chem. A* **125**, 3489 (2021).
- ¹⁰¹W. Jolly, K. Bomben, and C. Eyermann, *At. Data Nucl. Data Tables* **31**, 433 (1984).

Supplementary Information for:

**Chemical Space-Informed Machine Learning
Models for Rapid Predictions of X-ray
Photoelectron Spectra of Organic Molecules**

Susmita Tripathy, Surajit Das, Shweta Jindal, and Raghunathan Ramakrishnan*

Tata Institute of Fundamental Research, Hyderabad 500046, India

E-mail: ramakrishnan@tifrh.res.in

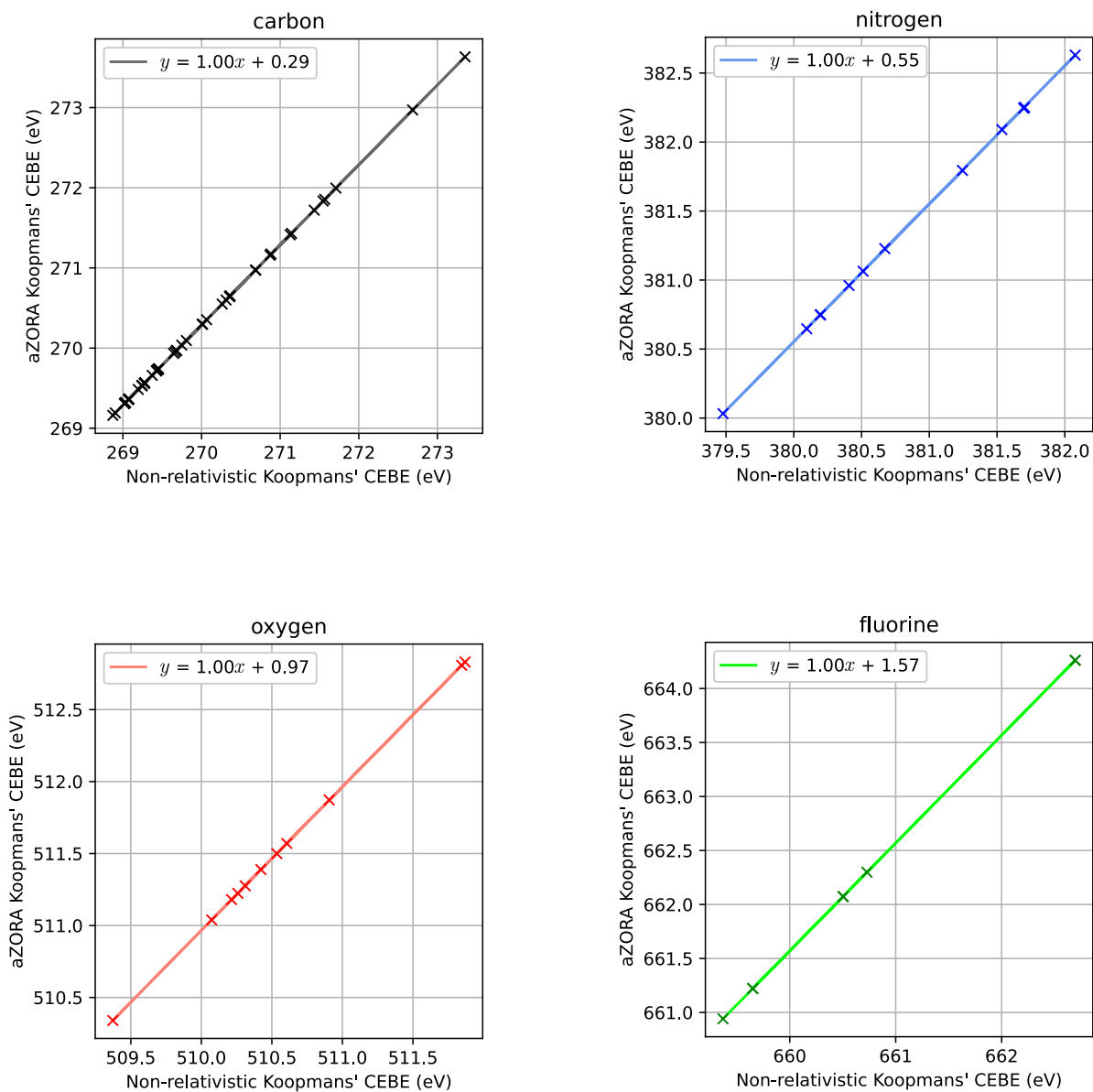


Figure S1: Systematic effect of aZORA correction on $1s$ -CEBEs (E_b^{1s}) of CONF atoms shown by straight-line fitting of non-relativistic values to aZORA values. The effect is shown for the baseline for Δ -ML, Koopmans' predicted E_b^{1s} for the first 32 molecules (excluding O_2) from bigQM7 ω at the PBE/cc-pVDZ level using geometries at the UFF level. As the slopes in all plots are nearly unity, as expected for atom-level corrections, aZORA values can be obtained using non-relativistic values by adding the intercept 0.29/0.55/0.97/1.57 eV for C/O/N/F atoms, respectively.

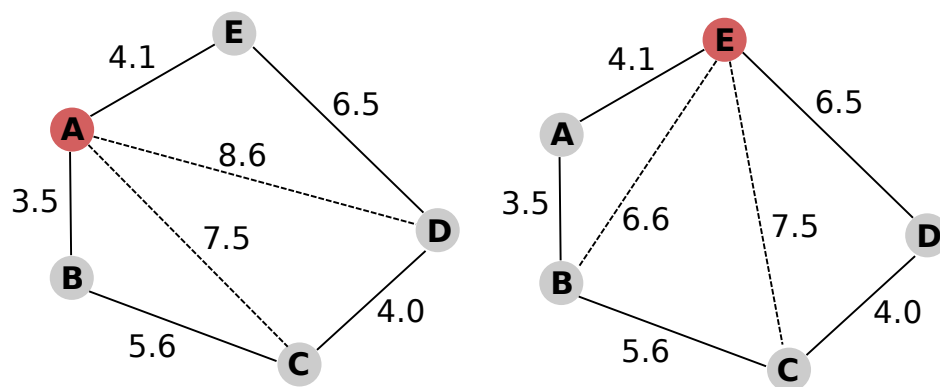


Figure S2: Sorting of atomic indices in the ACM (atomic Coulomb matrix) representation for a schematic molecule. For query atoms shown in red circles, A (left) and E (right), neighboring atoms with increasing interatomic distances are [B, E, C, D] and [A, D, B, C], respectively.

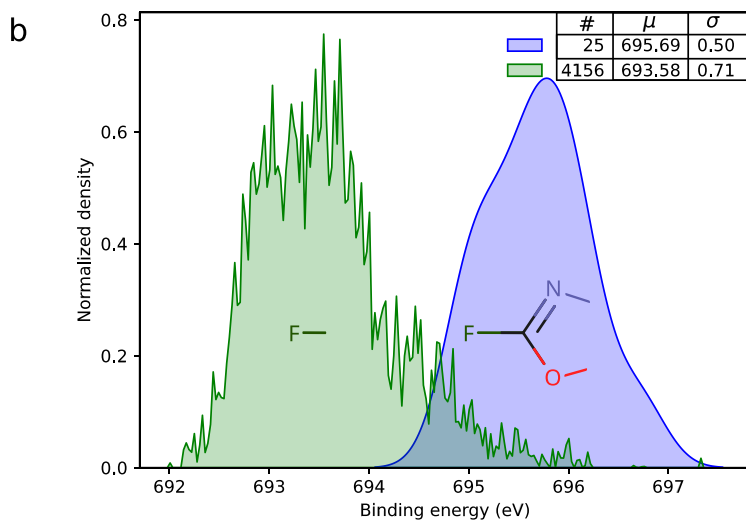
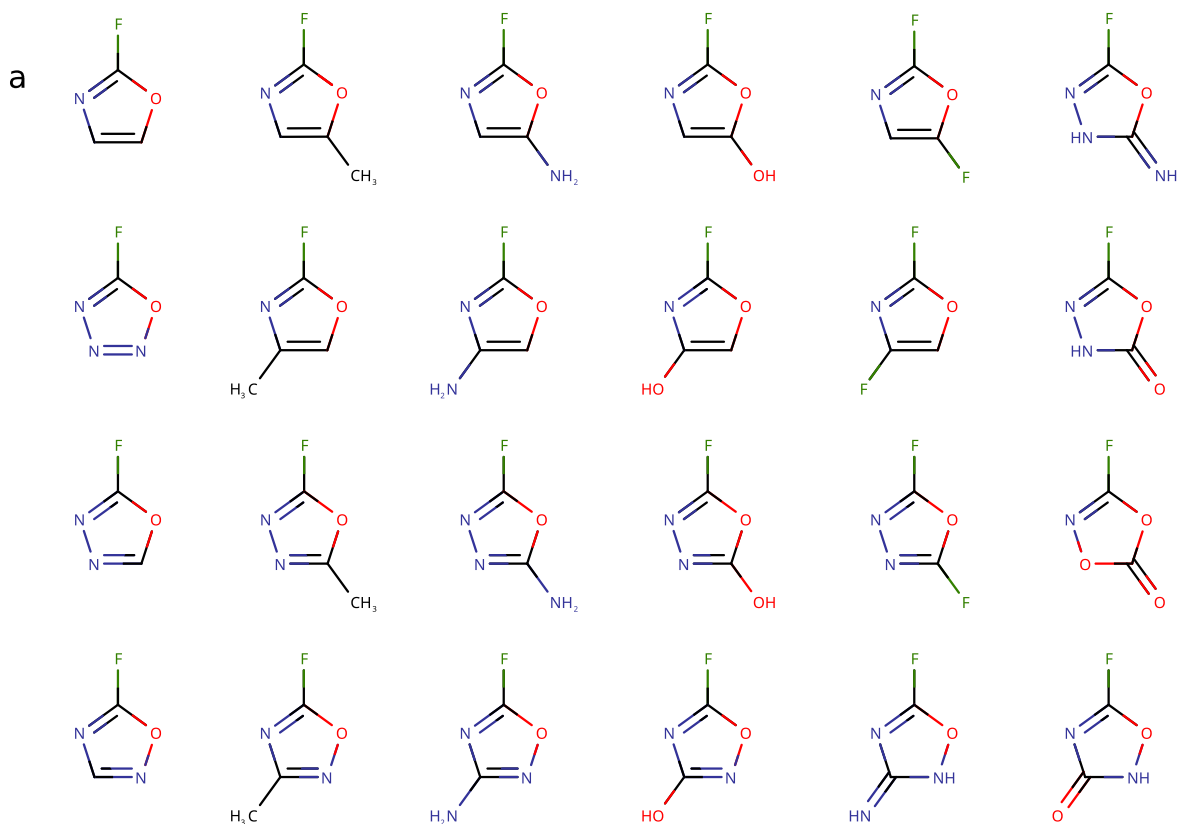


Figure S3: a) Five membered molecules with F atoms in the identical atomic environment, F-C(O-)(=N-). b) Distributions of E_b^{1s} are shown for all F atoms in bigQM7 ω (in green, bin width 0.05) and F atoms in the subset of bigQM7 ω with the common substructure shown in panel-a (in blue, bin width 1.0). In the legend, #, μ , and σ indicate the count, mean (in eV), and standard deviation (in eV), respectively. The area under each density curve integrates to #.

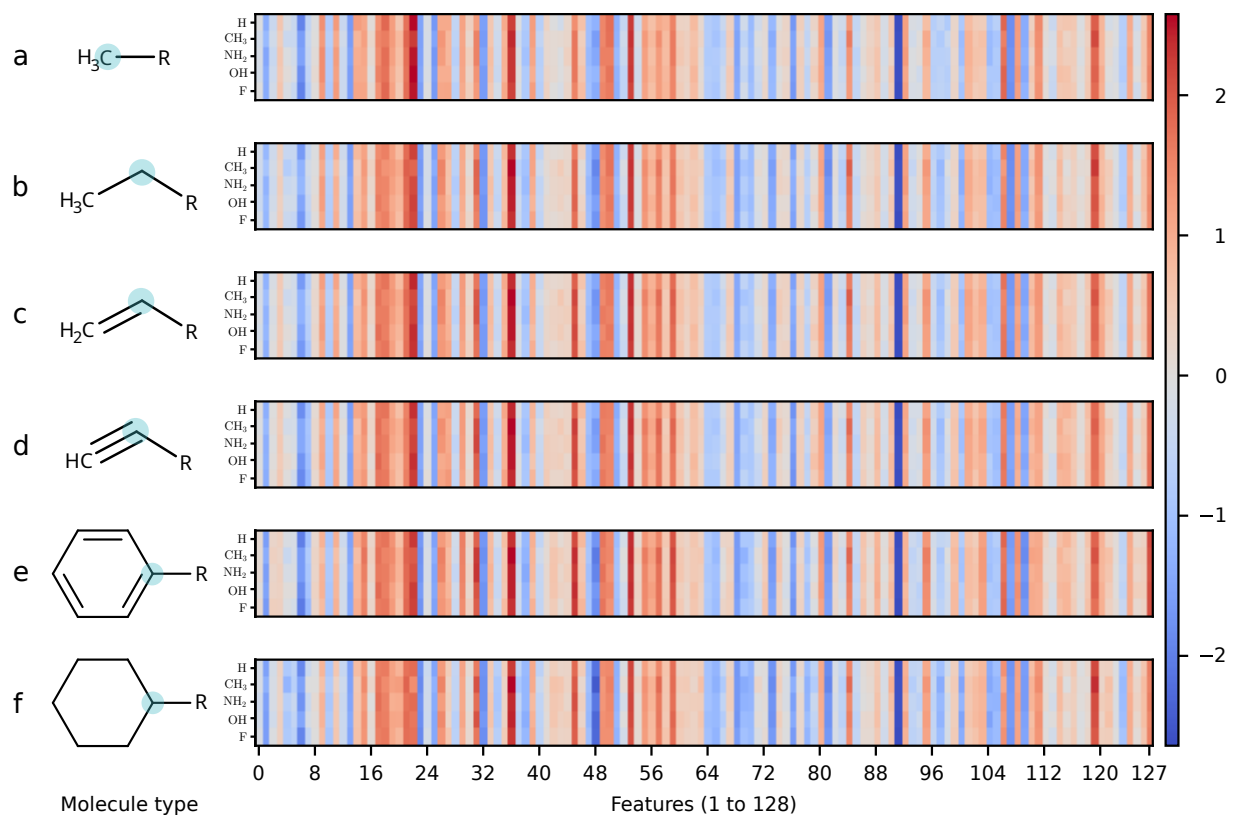


Figure S4: For six representative classes of molecules AtmEnv vectors of the highlighted ‘C’ atom are color coded: a) methane ($\text{CH}_3\text{-R}$), b) ethane ($\text{CH}_3\text{CH}_2\text{-R}$), c) ethylene ($\text{CH}_2\text{CH-R}$), d) acetylene (HC-R), e) benzene ($\text{C}_6\text{H}_5\text{-R}$), and f) cyclohexane ($\text{C}_6\text{H}_{11}\text{-R}$). For each class of molecule, five derivatives are considered with $\text{R}=\text{H}$, $-\text{CH}_3$, $-\text{NH}_2$, $-\text{OH}$, and $-\text{F}$, and AtmEnv vectors are plotted as five rows. Identical values for a given element of the vectors of different molecules indicate the presence of similar chemical environment.

Figure S5: Screenshots demonstrating the use of `cebeconf` within a Jupyter notebook. This notebook is provided in the project’s repository in the directory `example_query`. a) Install `cebeconf` and load all the pre-trained models using the function `calc_be`; b) and c) show direct-ML predictions (keyword ‘direct’) for ACM and AtmEnv representations, using keywords ‘ACM’ and ‘AtmEnv’ respectively, for a geometry ‘test.xyz’; d) and e) show Δ -ML predictions (keyword ‘delta’) for ACM and AtmEnv, respectively, for which baseline energies at PBE/cc-pVDZ level must be provided as a list in the input in the same order as the CONF atoms in the xyz file. In a), b), c), and e), the code produces an output spectrum by summing Gaussian functions at the predicted binding energies. Δ -ML predictions can also be made without providing baseline values as input if required, as shown in f), and the baseline values can be added separately, as shown in g) to estimate CEBEs at the target level. For brevity, we have omitted the module’s header from the output.

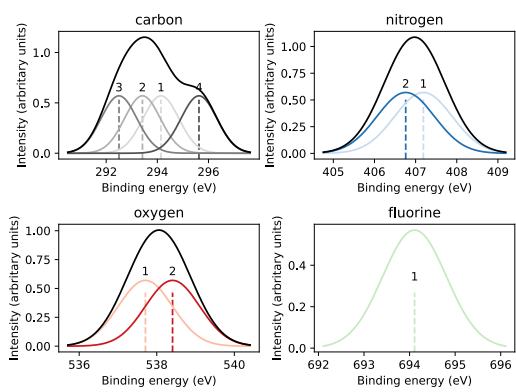
```
a) #Installation
!pip3 install cebeconf

from cebeconf import calc_be
```

```
b) calc_be('test.xyz','direct', 'ACM')
```

```
+-----+
| User inputs: |
+-----+
Reading coordinates from: test.xyz
Predicting 1s CEBEs using direct ML with the ACM descriptor

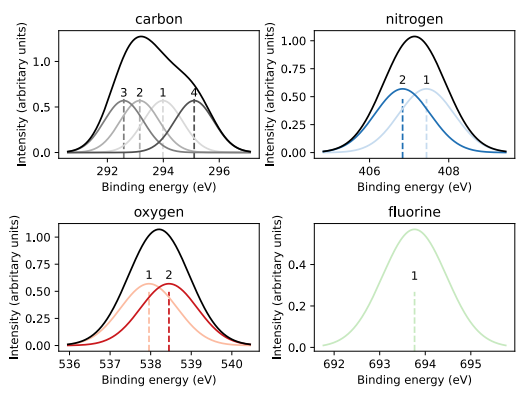
+-----+
| Prediction:  |
+-----+
1 C  -0.87732000    1.04762000    -0.00132000    294.14 eV
2 O  -1.66681000    1.97624000    -0.00242000    537.71 eV
3 C  -1.34390000    -0.26856000    0.00096000     293.42 eV
4 F  -2.67425000    -0.53668000    0.00204000     694.11 eV
5 C  -0.41740000    -1.31078000    0.00215000     292.50 eV
6 N   0.91481000    -1.04180000    0.00126000     407.19 eV
7 C   1.36896000     0.25355000    -0.00091000     295.63 eV
8 O   2.56676000     0.48016000    -0.00159000     538.41 eV
9 N   0.47290000     1.29324000    -0.00228000     406.76 eV
```



```
c) calc_be('test.xyz','direct', 'AtmEnv')
```

```
+-----+
| User inputs: |
+-----+
Reading coordinates from: test.xyz
Predicting 1s CEBEs using direct ML with the AtmEnv descriptor

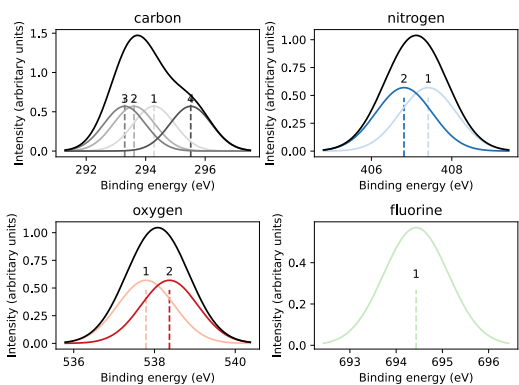
+-----+
| Prediction:  |
+-----+
1 C  -0.87732000    1.04762000    -0.00132000    293.99 eV
2 O  -1.66681000    1.97624000    -0.00242000    537.96 eV
3 C  -1.34390000    -0.26856000    0.00096000     293.16 eV
4 F  -2.67425000    -0.53668000    0.00204000     693.77 eV
5 C  -0.41740000    -1.31078000    0.00215000     292.59 eV
6 N   0.91481000    -1.04180000    0.00126000     407.44 eV
7 C   1.36896000     0.25355000    -0.00091000     295.10 eV
8 O   2.56676000     0.48016000    -0.00159000     538.45 eV
9 N   0.47290000     1.29324000    -0.00228000     406.83 eV
```



```
d) calc_be('test.xyz', 'delta', 'ACM', [272.44, 510.77, 272.21, 662.82, 271.86, 383.90, 273.48, 510.94, 383.33])
```

```
+-----+
| User inputs: |
+-----+
Reading coordinates from: test.xyz
Baseline energies at PBE-cc-pVDZ level of theory : [272.44, 510.77, 272.21,
662.82, 271.86, 383.9, 273.48, 510.94, 383.33]
Predicting 1s CEBEs using delta ML with the ACM descriptor
```

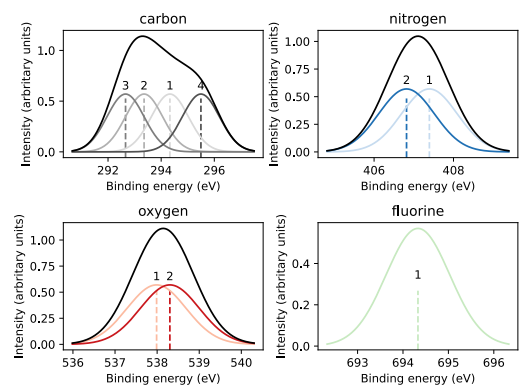
```
+-----+
| Prediction: |
+-----+
  1 C  -0.87732000    1.04762000   -0.00132000    294.28 eV
  2 O  -1.66681000    1.97624000   -0.00242000    537.79 eV
  3 C  -1.34390000   -0.26856000    0.00096000    293.61 eV
  4 F  -2.67425000   -0.53668000    0.00204000    694.43 eV
  5 C  -0.41740000   -1.31078000    0.00215000    293.29 eV
  6 N   0.91481000   -1.04180000    0.00126000    407.41 eV
  7 C   1.36896000    0.25355000   -0.00091000    295.52 eV
  8 O   2.56676000    0.48016000   -0.00159000    538.37 eV
  9 N   0.47290000    1.29324000   -0.00228000    406.81 eV
```



```
e) calc_be('test.xyz', 'delta', 'AtmEnv', [272.44, 510.77, 272.21, 662.82, 271.86, 383.90, 273.48, 510.94, 383.33])
```

```
+-----+
| User inputs: |
+-----+
Reading coordinates from: test.xyz
Baseline energies at PBE-cc-pVDZ level of theory : [272.44, 510.77, 272.21,
662.82, 271.86, 383.9, 273.48, 510.94, 383.33]
Predicting 1s CEBEs using delta ML with the AtmEnv descriptor
```

```
+-----+
| Prediction: |
+-----+
  1 C  -0.87732000    1.04762000   -0.00132000    294.33 eV
  2 O  -1.66681000    1.97624000   -0.00242000    537.99 eV
  3 C  -1.34390000   -0.26856000    0.00096000    293.36 eV
  4 F  -2.67425000   -0.53668000    0.00204000    694.33 eV
  5 C  -0.41740000   -1.31078000    0.00215000    292.66 eV
  6 N   0.91481000   -1.04180000    0.00126000    407.39 eV
  7 C   1.36896000    0.25355000   -0.00091000    295.50 eV
  8 O   2.56676000    0.48016000   -0.00159000    538.30 eV
  9 N   0.47290000    1.29324000   -0.00228000    406.82 eV
```



```
f) calc_be('test.xyz', 'delta', 'AtmEnv')
```

```
+-----+
| User inputs: |
+-----+
Reading coordinates from: test.xyz
Predicting 1s CEBEs using delta ML with the AtmEnv descriptor
```

```
+-----+
| Prediction: |
+-----+
  1 C  -0.87732000    1.04762000   -0.00132000    21.89 eV
  2 O  -1.66681000    1.97624000   -0.00242000    27.22 eV
  3 C  -1.34390000   -0.26856000    0.00096000    21.15 eV
  4 F  -2.67425000   -0.53668000    0.00204000    31.51 eV
  5 C  -0.41740000   -1.31078000    0.00215000    20.80 eV
  6 N   0.91481000   -1.04180000    0.00126000    23.49 eV
  7 C   1.36896000    0.25355000   -0.00091000    22.02 eV
  8 O   2.56676000    0.48016000   -0.00159000    27.36 eV
  9 N   0.47290000    1.29324000   -0.00228000    23.49 eV
```

```
g) delta_predictions = np.array(calc_be('test.xyz', 'delta', 'AtmEnv'))
   baseline_energies = np.array([272.44, 510.77, 272.21, 662.82, 271.86, 383.9, 273.48, 510.94, 383.33])
   predicted_energies = delta_predictions + baseline_energies
   print(predicted_energies)
```

```
[294.33 537.99 293.36 694.33 292.66 407.39 295.5 538.3 406.82]
```

Table S1: Splitting of six E_b^{1s} values in benzene (in eV) calculated using Koopmans, $G_{\Delta H}W_0$, and Δ -SCF approximations. For reference, the final column includes the experimental data.¹ The deviations are calculated from the minimum values (base) collected in the bottom row. Δ -SCF calculation is performed with SCAN/Tight-Full, whereas Koopmans and GW calculations are performed at the PBE/cc-pV5Z DFT level.

	Koopmans	$G_{\Delta H}W_0$	Δ -SCF	Expt. ¹
	0.023	0.105	0.000	0.064
	0.017	0.034	0.000	0.048
	0.017	0.034	0.000	0.048
	0.006	0.023	0.000	0.016
	0.006	0.021	0.000	0.016
	0.000	0.000	0.000	0.000
base	269.29	290.09	290.29	290.26

Table S2: Number of molecules with C, N, O, F atoms in the bigQM7 ω dataset along with the number of entries (#) of E_b^{1s} . The number of molecules converged in Δ -SCF calculations is also given.

Element	Molecules	Converged Molecules	$\#E_b^{1s}$
C	12875	12674	56066
N	8486	8368	15071
O	7774	7628	10544
F	3256	3230	4156
all	12880	12679	85837

Table S3: Variation of out-of-sample MAE (in eV) for direct-ML and Δ -ML with the length of AtmEnv feature vector.

	MAE (eV)			
Length	128	256	512	1024
direct-ML	0.097	0.087	0.080	0.076
Δ -ML	0.050	0.046	0.044	0.043

Table S4: $G_{\Delta H}W_0$ estimated E_b^{1s} using cc-pVnZ (n=T,Q,5) basis sets, and values extrapolated at the complete basis set (CBS) limit. Accuracy of a straight line fitted to the cc-pVnZ (n=T,Q,5) energies compared to CBS are quantified through mean absolute error (MAE) and coefficient of determination, R^2 . In the cases where the trend in binding energies is non-monotonic, we have taken the BE obtained using cc-pV5Z instead of CBS energy, denoted by a †. The first and last atom of three-membered cyclic molecules (last 9 entries) are linked to each other, this is denoted by -. For chemically equivalent atoms in a molecule, the KS state denoted with *, corresponding to maximum Mulliken population, is selected as the reference in TABLE I. See, IIB of the article for more details.

Molecule	Atom	cc-pVTZ	cc-pVQZ	cc-pV5Z	CBS	MAE(eV)	R^2
CH ₄	C	290.201	290.479	290.610	290.761	0.00	1.00
NH ₃	N	404.703	405.367	405.398	405.766	0.07	0.94
H ₂ O	O	539.528	539.630	539.506	539.505†		
HF	F	694.123	694.014	693.922	693.852	0.01	0.97
H ₃ C-CH ₃	C	290.093	290.381	290.510	290.671*	0.00	1.00
		290.079	290.391	290.506	290.680	0.01	1.00
H ₂ N-CH ₃	C	290.880	291.205	291.164	291.164†		
H ₂ N-CH ₃	N	404.765	404.941	405.060	405.136	0.02	0.97
HO-CH ₃	C	291.726	292.067	292.268	292.468	0.02	0.99
HO-CH ₃	O	538.828	538.917	538.905	538.905†		
F-CH ₃	C	292.757	293.107	293.251	293.518	0.02	0.99
F-CH ₃	F	692.737	692.677	692.637	692.588	0.00	1.00
F ₂	F	696.959	696.801	696.706	696.588*	0.01	1.00
		696.965	696.807	696.735	696.621	0.00	1.00
H ₂ C=CH ₂	C	290.306	290.601	290.701	290.872*	0.01	1.00
		290.266	290.552	290.637	290.802	0.01	0.99
H ₂ C=O	C	293.772	294.130	294.275	294.498	0.00	1.00
H ₂ C=O	O	539.235	539.314	539.370	539.420	0.01	0.99
HC≡CH	C	290.695	290.942	291.116	291.274*	0.02	0.99
		290.622	290.928	291.027	291.216	0.01	1.00

H ₃ C-CH ₂ -CH ₃	-CH ₃	289.903	290.226	290.305	290.487*	0.02	0.99
		289.903	290.199	290.272	290.439	0.02	0.99
H ₃ C-CH ₂ -CH ₃	-CH ₂ -	290.025	290.367	290.421	290.612	0.03	0.97
H ₃ C-CH ₂ -NH ₂	H ₃ C-	289.940	290.272	290.357	290.546	0.02	0.99
H ₃ C-CH ₂ -NH ₂	-CH ₂ -	290.788	291.118	291.305	291.496	0.01	1.00
H ₃ C-CH ₂ -NH ₂	N	404.457	404.702	404.836	404.977	0.01	1.00
H ₃ C-CH ₂ -OH	H ₃ C-	290.185	290.527	290.618	290.815	0.02	0.99
H ₃ C-CH ₂ -OH	-CH ₂ -	291.580	291.925	292.065	292.266	0.00	1.00
H ₃ C-CH ₂ -OH	O	538.472	538.568	538.646	538.703	0.01	0.97
H ₃ C-CH ₂ -F	H ₃ C-	290.470	290.808	290.919	291.118	0.01	1.00
H ₃ C-CH ₂ -F	-CH ₂ -	292.490	292.866	292.999	293.221	0.01	1.00
H ₃ C-CH ₂ -F	F	692.194	692.151	692.124	692.098	0.00	0.99
F ₂ CH ₂	C	295.335	295.736	295.867	296.123	0.02	0.99
F ₂ CH ₂	F	693.499	693.458	693.433	693.406*	0.00	0.99
		693.498	693.457	693.433	693.406	0.00	1.00
H ₃ C-NH-CH ₃	N	404.501	404.699	404.671	404.671†		
H ₃ C-NH-CH ₃	C	290.709	291.029	291.116	291.298	0.02	0.99
		290.709	291.033	291.132	291.317	0.01	0.99
H ₃ C-O-CH ₃	O	538.389	538.451	538.437	538.437†		
H ₃ C-O-CH ₃	C	291.534	291.870	292.010	292.206*	0.00	1.00
		291.534	291.868	291.944	292.137	0.02	0.98
H ₃ C-HC=CH ₂	H ₃ C-	290.215	290.518	290.543	290.716	0.03	0.95
H ₃ C-HC=CH ₂	-HC=	290.157	290.451	290.557	290.728	0.01	1.00
H ₃ C-HC=CH ₂	=CH ₂	289.692	289.985	290.094	290.264	0.01	1.00
H ₃ C-HC=O	H ₃ C-	290.786	291.104	291.295	291.491	0.01	0.99
H ₃ C-HC=O	-HC	293.202	293.556	293.726	293.941	0.00	1.00
H ₃ C-HC=O	O	538.249	538.341	538.478	538.539	0.03	0.89

H ₃ C-C≡N	H ₃ C-	292.045	292.388	292.491	292.703	0.01	0.99
H ₃ C-C≡N	-C≡	291.927	292.167	292.288	292.438	0.00	1.00
H ₃ C-C≡N	N	404.988	405.238	405.399	405.558	0.01	0.99
H ₂ N-HC=NH	H ₂ N-	405.610	405.821	406.064	406.199	0.04	0.93
H ₂ N-HC=NH	C	292.153	292.520	292.668	292.890	0.00	1.00
H ₂ N-HC=NH	=NH	403.631	403.870	403.956	404.100	0.01	1.00
H ₂ N-HC=O	N	405.859	406.262	406.325	406.569	0.03	0.97
H ₂ N-HC=O	C	293.389	293.750	293.808	294.028	0.03	0.97
H ₂ N-HC=O	O	537.223	537.336	537.447	537.521	0.02	0.96
HO-HC=O	HO-	540.369	540.477	540.539	540.611	0.00	1.00
HO-HC=O	C	294.668	295.039	295.194	295.433	0.00	1.00
HO-HC=O	=O	538.471	538.577	538.701	538.774	0.02	0.93
F-HC=CH ₂	F	693.045	693.015	692.998	692.979	0.00	1.00
F-HC=CH ₂	-HC=	292.686	293.044	293.126	293.345	0.02	0.98
F-HC=CH ₂	=CH ₂	290.306	290.627	290.664	290.859	0.03	0.96
H ₂ N-N=CH ₂	H ₂ N-	405.472	406.000	406.121	406.437	0.03	0.98
H ₂ N-N=CH ₂	-N=	405.746	405.985	406.089	406.233	0.00	1.00
H ₂ N-N=CH ₂	C	290.541	290.863	291.018	291.214	0.00	1.00
HO-N=CH ₂	O	539.580	539.679	539.724	539.786	0.00	1.00
HO-N=CH ₂	N	406.674	406.921	407.092	407.250	0.02	0.99
HO-N=CH ₂	C	291.138	291.468	291.628	291.835	0.00	1.00
H ₃ C-C≡CH	H ₃ C	291.061	291.396	291.502	291.703	0.01	0.99
H ₃ C-C≡CH	-C≡	290.287	290.502	290.681	290.815	0.02	0.97
H ₃ C-C≡CH	≡CH	289.727	289.968	289.943	290.083	0.04	0.85
-CH ₂ -CH ₂ -CH ₂ -	C	290.117	290.419	290.552	290.728*	0.00	1.00
		290.117	290.419	290.552	290.728	0.00	1.00
		290.142	290.402	290.568	290.721	0.02	0.99

-CH ₂ -CH ₂ -NH-	C	291.001	291.301	291.433	291.611*	0.00	1.00
		290.983	291.274	291.446	291.620	0.01	0.99
-CH ₂ -CH ₂ -NH-	N	404.971	405.136	405.180	405.277	0.01	0.99
-CH ₂ -CH ₂ -O-	C	291.873	292.223	292.276	292.484*	0.03	0.97
		291.854	292.178	292.351	292.549	0.01	1.00
-CH ₂ -CH ₂ -O-	O	538.783	538.853	538.989	539.036	0.03	0.85

Table S5: Summary of non-converged systems in the bigQM7 ω dataset. Cations with a 1s-hole that fail to converge during the SCF procedure are labeled as 'Non-converged atoms.' Molecules containing one or more non-converged atoms are denoted 'Non-converged molecules.' The percentage relative to the total number of atoms/molecules in the bigQM7 ω dataset is provided in parentheses. A breakdown of the atoms by hybridization is also included.

Quantity	C	N	O	F	all
Non-converged molecules (%)	201 (1.56)	118 (1.39)	146 (1.88)	26 (0.80)	201 (1.56)
Non-converged atoms (%)	116 (0.20)	28 (0.18)	65 (0.60)	9 (0.22)	218 (0.25)
Distribution (sp^3, sp^2, sp)	(29,84,3)	(2,25,1)	(2,63,-)	(9,-,-)	(42,172,4)

Table S6: Details of 201 molecules exhibiting failure in SCF convergence for core-ionized cations. The column Molecule id denotes the title of the molecule in the XYZ format collected in the bigQM7 ω dataset. SMILES representation and index of atoms for which core-ionized cations exhibiting convergence failure are also provided.

Molecule id	SMILES	Atomic index
bigQM7 ω -000312	CNCC=O	5
bigQM7 ω -000339	C=CNC=N	4
bigQM7 ω -000604	CNCC(C)=O	4
bigQM7 ω -000635	CC(=O)CC=O	5
bigQM7 ω -000649	CC(=N)NC=C	2
bigQM7 ω -000670	NC(=N)ON=C	5
bigQM7 ω -000836	CC(=C)C(C)=C	1,5

bigQM7 ω _000841	<chem>CC(=C)C(F)=C</chem>	5
bigQM7 ω _001073	<chem>ON(C=C)C=N</chem>	5
bigQM7 ω _001162	<chem>NCC(=C)C=C</chem>	1
bigQM7 ω _001163	<chem>OCC(=C)C=C</chem>	2
bigQM7 ω _001166	<chem>FCC(=C)C=C</chem>	2
bigQM7 ω _001173	<chem>OCC(=O)C=O</chem>	6
bigQM7 ω _001193	<chem>COC(=C)C=O</chem>	6
bigQM7 ω _001220	<chem>C=CC(=O)C=O</chem>	5,6
bigQM7 ω _001485	<chem>O=c1nn[nH]o1</chem>	4
bigQM7 ω _001736	<chem>CCNCC=O</chem>	6
bigQM7 ω _001754	<chem>C=CCCC=O</chem>	6
bigQM7 ω _001756	<chem>O=CCCC=O</chem>	1,2,5,6
bigQM7 ω _001775	<chem>C=NOCC=O</chem>	2
bigQM7 ω _001838	<chem>ON=CCC=O</chem>	5
bigQM7 ω _001867	<chem>ON=CON=C</chem>	5
bigQM7 ω _001962	<chem>O=CC=CC=O</chem>	5
bigQM7 ω _002038	<chem>O=CC1CNC1</chem>	2
bigQM7 ω _002041	<chem>O=CC1COC1</chem>	2
bigQM7 ω _002540	<chem>CN(C)CC(O)=O</chem>	5
bigQM7 ω _002552	<chem>CC(=O)CC(C)=O</chem>	2,5
bigQM7 ω _002554	<chem>CC(=O)CC(N)=O</chem>	2
bigQM7 ω _002765	<chem>CC(F)(CO)C=O</chem>	6
bigQM7 ω _002830	<chem>FC(F)(C=O)C=O</chem>	7
bigQM7 ω _002945	<chem>CC(N)CON=C</chem>	7
bigQM7 ω _003062	<chem>CC(=C)CCC=O</chem>	7
bigQM7 ω _003065	<chem>CC(=O)CCC=O</chem>	7
bigQM7 ω _003077	<chem>FC(=C)CCC=O</chem>	7

bigQM7 ω _003094	NC(=O)CNN=C	6
bigQM7 ω _003099	CC(=O)COC=C	2
bigQM7 ω _003112	NC(=O)CON=C	7
bigQM7 ω _003125	NC(=O)NCC=O	7
bigQM7 ω _003136	CC(=O)NOC=O	6
bigQM7 ω _003416	CC(=C)C=CC=O	1
bigQM7 ω _003419	CC(=O)C=CC=O	6
bigQM7 ω _003422	NC(=N)C=CC=O	7
bigQM7 ω _003431	FC(=C)C=CC=O	1
bigQM7 ω _003432	FC(=C)C=CC#N	1
bigQM7 ω _003521	FC(=C)C#CC=C	1
bigQM7 ω _003990	CC(CN)ON=C	6
bigQM7 ω _004072	COCC(F)C=O	6
bigQM7 ω _004115	CC(CC=O)C=O	4
bigQM7 ω _004123	OC(CC=C)C=O	7
bigQM7 ω _004125	OC(CC=O)C=O	5,7
bigQM7 ω _004132	FC(CC=C)C=O	7
bigQM7 ω _004142	CC(NC=O)C=O	7
bigQM7 ω _004160	CN(CC=O)C=O	5
bigQM7 ω _004187	FC(CC#C)C=O	7
bigQM7 ω _004437	CCC(=N)NC=C	3
bigQM7 ω _004446	FCC(=N)NC=C	3
bigQM7 ω _004522	CNC(=N)ON=C	7
bigQM7 ω _004523	NNC(=N)ON=C	6
bigQM7 ω _004564	CNCC(=C)C=C	2
bigQM7 ω _004565	CNCC(=C)C=O	7
bigQM7 ω _004569	CNCC(=O)C#N	7

bigQM7 ω _004570	<chem>COCC(=C)C=C</chem>	3
bigQM7 ω _004580	<chem>CCNC(=O)C=O</chem>	7
bigQM7 ω _004589	<chem>CON=C(N)C=O</chem>	7
bigQM7 ω _004595	<chem>CCOC(=C)C=O</chem>	7
bigQM7 ω _004602	<chem>C=CC(=C)CC#N</chem>	6
bigQM7 ω _004605	<chem>C=C(CC=O)C=O</chem>	5
bigQM7 ω _004614	<chem>O=CCC(=O)C=O</chem>	5
bigQM7 ω _004618	<chem>C=CC(=C)NC=N</chem>	7
bigQM7 ω _004619	<chem>C=CC(=C)NC=O</chem>	7
bigQM7 ω _004627	<chem>C=CNC(=N)C=O</chem>	6
bigQM7 ω _004631	<chem>N=C(NC=O)C=O</chem>	6
bigQM7 ω _004674	<chem>CNCC(=O)C#C</chem>	4
bigQM7 ω _004693	<chem>C=CNC(=N)C#C</chem>	4
bigQM7 ω _004842	<chem>CN=CN(N)C=C</chem>	3
bigQM7 ω _004880	<chem>CCC(=C)C=CC</chem>	1
bigQM7 ω _004948	<chem>CC=CC(=C)C=O</chem>	7
bigQM7 ω _004959	<chem>FC=CC(=O)C=O</chem>	7
bigQM7 ω _005027	<chem>CC#CC(=O)C=O</chem>	7
bigQM7 ω _005089	<chem>FC=C(F)CC=O</chem>	7
bigQM7 ω _005093	<chem>CC(CC=O)=NO</chem>	4
bigQM7 ω _005120	<chem>CC(ON=C)=NO</chem>	4
bigQM7 ω _005271	<chem>CC(C=C)=CCO</chem>	1
bigQM7 ω _005272	<chem>CC(C=C)=CCF</chem>	1
bigQM7 ω _005293	<chem>COC=C(C)C=C</chem>	1
bigQM7 ω _005307	<chem>CC(C=C)=CC#N</chem>	1
bigQM7 ω _005315	<chem>NC(C=C)=CC#N</chem>	3
bigQM7 ω _005317	<chem>NC(=CC=O)C#N</chem>	6

bigQM7 ω _005668	CC(C=O)C(F)=C	3
bigQM7 ω _005705	FC(C=O)C(F)=C	4
bigQM7 ω _005709	CN(C=C)C(C)=N	5
bigQM7 ω _005723	CC(=N)N(N)C=C	2
bigQM7 ω _005896	CC(O)C(=C)C=C	2,3
bigQM7 ω _005965	CCC(=C)C(F)=C	6
bigQM7 ω _005982	OCC(=O)C(O)=O	5
bigQM7 ω _005991	CC(=O)C(=N)NO	2
bigQM7 ω _006035	CC(=C)C(=C)C#N	1
bigQM7 ω _006052	CC(=C)C(=O)C=O	7
bigQM7 ω _006058	NC(=N)C(=O)C=O	5,7
bigQM7 ω _006064	OC(=O)C(=O)C=O	5
bigQM7 ω _006294	CC1(CNC1)C=O	6
bigQM7 ω _006304	CC1(COC1)C=O	6
bigQM7 ω _006311	FC1(COC1)C=O	6
bigQM7 ω _006586	O=C1CNC(=O)C1	2
bigQM7 ω _006653	CC1CC(=C)C=C1	1
bigQM7 ω _006671	CN1CC(=C)C=N1	1
bigQM7 ω _006704	C=C1NC(=N)C=C1	4,7
bigQM7 ω _006709	C=C1NC(=N)N=C1	6
bigQM7 ω _006715	C=C1OC(=C)C=C1	7
bigQM7 ω _006956	CC1=CC(N)C=C1	1
bigQM7 ω _006959	OC1C=CC(F)=C1	6
bigQM7 ω _006961	FC1C=CC(F)=C1	6
bigQM7 ω _007033	CC1=CC(=O)C=N1	5
bigQM7 ω _007036	NC1=CC(=N)N=C1	6
bigQM7 ω _007476	O=C1COC=CC1	2

bigQM7 ω _007576	C=C1CCCC=C1	3
bigQM7 ω _007587	C=C1COCC=C1	3
bigQM7 ω _007601	CC1CC=CC=C1	1
bigQM7 ω _007637	Nc1cncnn1	4
bigQM7 ω _007709	O=c1cn[nH]nn1	7
bigQM7 ω _007961	O=C1CCCC1=O	1,7
bigQM7 ω _007970	N=C1NCCC1=O	7
bigQM7 ω _007980	C=C1CCOC1=C	5
bigQM7 ω _008035	FC1CC=CC1=C	1
bigQM7 ω _008060	Nn1[nH]ncc1=N	5
bigQM7 ω _008063	On1[nH]ncc1=O	5
bigQM7 ω _008071	Cn1[nH]nnc1=O	5
bigQM7 ω _008073	Nn1[nH]nnc1=O	5
bigQM7 ω _008082	Cn1oncc1=N	4
bigQM7 ω _008097	Nn1onnc1=O	4
bigQM7 ω _008195	C=C1CC=CC1=C	5
bigQM7 ω _008202	O=C1NC=CC1=O	2
bigQM7 ω _008206	O=C1NN=CC1=O	2
bigQM7 ω _008207	C=C1N=CNC1=N	6
bigQM7 ω _008209	N=C1NC=NC1=N	4
bigQM7 ω _008212	C=C1OC=CC1=C	2,4,6
bigQM7 ω _008254	FC1=CCCC1=C	1
bigQM7 ω _008403	CC1=NC=CC1=O	7
bigQM7 ω _008759	O=CNC1CNC1	2
bigQM7 ω _008760	C=NNC1CNC1	2
bigQM7 ω _008898	NC1CC1OC=O	6
bigQM7 ω _008908	CC1NC1CC=O	6,7

bigQM7 ω _009003	CC(=O)C1CNC1	2
bigQM7 ω _009005	NC(=O)C1CNC1	2
bigQM7 ω _009367	CNC(C=O)C#N	5
bigQM7 ω _009421	O=CC(C=O)C#N	5
bigQM7 ω _009441	O=CC(C=O)C#C	5
bigQM7 ω _009591	CNC(C=O)=NC	5
bigQM7 ω _009831	CCOCCC=O	7
bigQM7 ω _009837	CCCNCC=O	7
bigQM7 ω _009844	FCCNCC=O	6
bigQM7 ω _009895	C=CCCCC=O	7
bigQM7 ω _009902	N=CNCCC=O	7
bigQM7 ω _009904	O=CCCNC=O	1
bigQM7 ω _009915	C=CCCOCN=C	6
bigQM7 ω _009916	C=NOCCC=O	1,2
bigQM7 ω _009921	C=COCON=C	7
bigQM7 ω _009963	O=CCOCC#C	1
bigQM7 ω _010050	FC=CCCC=O	7
bigQM7 ω _010054	ON=CCCC=O	7
bigQM7 ω _010081	NN=CNCC=C	7
bigQM7 ω _010105	NN=COCC=C	6
bigQM7 ω _010110	CC=NOCC=O	7
bigQM7 ω _010265	CNCC=CC=O	7
bigQM7 ω _010267	COCC=CC=C	1
bigQM7 ω _010268	COCC=CC=O	6
bigQM7 ω _010274	CNCC=NN=C	7
bigQM7 ω _010312	OCC=CCC=O	7
bigQM7 ω _010327	OCC=CNC=N	6

bigQM7 ω _010328	FCC=CNC=N	6
bigQM7 ω _010374	O=CCC=CC=O	6
bigQM7 ω _010406	C=NOC=NN=C	2
bigQM7 ω _010474	CC=CC=CC=C	1
bigQM7 ω _010546	COCC#CC=C	1
bigQM7 ω _010570	O=CCC#CC=O	6
bigQM7 ω _010575	O=CCC#CC#C	1
bigQM7 ω _010892	NCC1CN1N=C	6
bigQM7 ω _011104	O=CC1CC=NN1	1
bigQM7 ω _011113	O=CC1CC=NO1	2
bigQM7 ω _011115	C=CC1OC=CO1	2
bigQM7 ω _011178	ON=c1onno1	5
bigQM7 ω _011223	O=CC1COC=C1	1
bigQM7 ω _011229	O=CC1NCC=C1	2
bigQM7 ω _011236	C=CN1CCN=C1	7
bigQM7 ω _011349	N=Cn1cccc1	2
bigQM7 ω _011351	C=Nn1cccc1	2
bigQM7 ω _011389	O=Nc1cc[nH]c1	1
bigQM7 ω _011461	C=CC1=CCCC1	7
bigQM7 ω _011469	C=CC1=CCNC1	7
bigQM7 ω _011472	C=CC1=CCOC1	7
bigQM7 ω _011483	N#CC1=NCCN1	2
bigQM7 ω _011623	O=Cc1ncc[nH]1	2
bigQM7 ω _011638	O=Cc1ccno1	2
bigQM7 ω _011672	CCC1=CCC=C1	1
bigQM7 ω _011742	NCc1nnon1	5
bigQM7 ω _011879	OC(C=O)C1CN1	3

bigQM7 ω _011985	C=CC(=C)C1CO1	5,6
bigQM7 ω _011995	O=CC(=O)N1CC1	1
bigQM7 ω _012467	N1C=CC=NC=N1	2,4
bigQM7 ω _012468	N1C=NC=NC=N1	2
bigQM7 ω _012799	NC1C2NC1C=C2	2

References

- (1) Myrseth, V.; Børve, K.; Wiesner, K.; Bässler, M.; Svensson, S.; Sæthre, L. Vibrational structure and vibronic coupling in the carbon 1s photoelectron spectra of benzene and deuterobenzene. *Phys. Chem. Chem. Phys.* **2002**, *4*, 5937–5943.